

1 **Functional assessment of the “two-hit” model for neurodevelopmental defects**  
2 **in *Drosophila* and *X. laevis***

3  
4 Short title: Assessment of “two-hit” model for developmental defects

5  
6 Lucilla Pizzo<sup>1\*</sup>, Micaela Lasser<sup>2\*</sup>, Tanzeen Yusuff<sup>1</sup>, Matthew Jensen<sup>1</sup>, Phoebe Ingraham<sup>1</sup>, Emily  
7 Huber<sup>1</sup>, Mayanglambam Dhruva Singh<sup>1</sup>, Connor Monahan<sup>2</sup>, Janani Iyer<sup>1</sup>, Inshya Desai<sup>1</sup>,  
8 Siddharth Karthikeyan<sup>1</sup>, Dagny J. Gould<sup>1</sup>, Sneha Yennawar<sup>1</sup>, Alexis T Weiner<sup>1</sup>, Vijay Kumar  
9 Pounraja<sup>1</sup>, Arjun Krishnan<sup>4,5</sup>, Melissa Rolls<sup>1</sup>, Laura Anne Lowery<sup>6</sup> and Santhosh Girirajan<sup>1,3#</sup>

10

11 1. Department of Biochemistry and Molecular Biology, The Pennsylvania State University,  
12 University Park, PA USA

13 2. Department of Biology, Boston College, Chestnut Hill, MA USA

14 3. Department of Anthropology, The Pennsylvania State University, University Park, PA  
15 USA

16 4. Department of Computational Mathematics, Science and Engineering, Michigan State,  
17 University, East Lansing, MI, USA

18 5. Department of Biochemistry and Molecular Biology, Michigan State University, East  
19 Lansing, MI, USA

20 6. Department of Medicine, Boston University Medical Center, Boston, MA, USA

21

22 \*contributed equally to the work

23

24 **#Corresponding author:**

25 Santhosh Girirajan, MBBS, PhD

26 205A Life Sciences Building

27 Pennsylvania State University

28 University Park, PA 16802

29 E-mail: [sxg47@psu.edu](mailto:sxg47@psu.edu)

30 Phone: 814-865-0674

31

32 **Keywords:** phenotypic variability, modifier, CNV

33

## 34 **Abstract**

35 We previously identified a deletion on chromosome 16p12.1 that is mostly inherited and  
36 associated with multiple neurodevelopmental outcomes, where severely affected probands  
37 carried an excess of rare pathogenic variants compared to mildly affected carrier parents. We  
38 hypothesized that the 16p12.1 deletion sensitizes the genome for disease, while “second-hits” in  
39 the genetic background modulate the phenotypic trajectory. To test this model, we examined  
40 how neurodevelopmental defects conferred by knockdown of individual 16p12.1 homologs are  
41 modulated by simultaneous knockdown of homologs of “second-hit” genes in *Drosophila*  
42 *melanogaster* and *Xenopus laevis*. We observed that knockdown of 16p12.1 homologs affect  
43 multiple phenotypic domains, leading to delayed developmental timing, seizure susceptibility,  
44 brain alterations, abnormal dendrite and axonal morphology, and cellular proliferation defects.  
45 Compared to genes within the 16p11.2 deletion, which has higher *de novo* occurrence, 16p12.1  
46 homologs were less likely to interact with each other in *Drosophila* models or a human brain-  
47 specific interaction network, suggesting that interactions with “second-hit” genes confer higher  
48 impact towards neurodevelopmental phenotypes. Assessment of 212 pairwise interactions in  
49 *Drosophila* between 16p12.1 homologs and 76 homologs of patient-specific “second-hit” genes  
50 (such as *ARID1B* and *CACNA1A*), genes within neurodevelopmental pathways (such as *PTEN*  
51 and *UBE3A*), and transcriptomic targets (such as *DSCAM* and *TRRAP*) identified both interactive  
52 (63%) and additive (37%) effects. In 11 out of 15 families, homologs of patient-specific “second-  
53 hits” enhanced or suppressed the phenotypic effects of one or many 16p12.1 homologs. In fact,  
54 homologs of *SETD5* synergistically interacted with homologs of *MOSMO* in both *Drosophila*  
55 and *X. laevis*, leading to modified cellular and brain phenotypes, as well as axon outgrowth  
56 defects that were not observed with knockdown of either individual homolog. Our results suggest

57 that several 16p12.1 genes sensitize the genome towards neurodevelopmental defects, and  
58 complex interactions with “second-hit” genes determine the ultimate phenotypic manifestation.

59

## 60 **Author Summary**

61 Copy-number variants, or deletions and duplications in the genome, are associated with multiple  
62 neurodevelopmental disorders. The developmental delay-associated 16p12.1 deletion is mostly  
63 inherited, and severely affected children carry an excess of “second-hits” variants compared to  
64 mildly affected carrier parents, suggesting that additional variants modulate the clinical  
65 manifestation. We studied this “two-hit” model using *Drosophila* and *Xenopus laevis*, and  
66 systematically tested how homologs of “second-hit” genes modulate neurodevelopmental defects  
67 observed for 16p12.1 homologs. We observed that 16p12.1 homologs independently led to  
68 multiple neurodevelopmental features and had fewer interactions with each other, suggesting that  
69 interactions with “second-hit” homologs could have a higher impact towards  
70 neurodevelopmental defects than interactions between 16p12.1 homologs. We tested 212  
71 pairwise interactions of 16p12.1 homologs with “second-hit” homologs and genes within  
72 conserved neurodevelopmental pathways, and observed modulation of neurodevelopmental  
73 defects caused by 16p12.1 homologs in 11 out of 15 families studied, and 16/32 of these changes  
74 could be attributed to genetic interactions. Interestingly, we observed that *SETD5* homologs  
75 interacted with homologs of *MOSMO*, which conferred additional neuronal phenotypes not  
76 observed with knockdown of individual homologs. We propose that the 16p12.1 deletion  
77 sensitizes the genome to multiple neurodevelopmental defects, and complex interactions with  
78 “second-hit” genes determine the final manifestation.

## 79 **Introduction**

80 Rare recurrent copy-number variants (CNVs) account for about 15% of individuals with  
81 neurodevelopmental disorders, such as autism, intellectual disability, and schizophrenia (1, 2).  
82 While certain CNVs were initially associated with specific neuropsychiatric diagnoses, such as  
83 the 16p11.2 deletion and autism (3, 4), 3q29 deletion and schizophrenia (5), and 15q13.3  
84 deletion and epilepsy (6), variable expressivity of phenotypes has been the norm rather than the  
85 exception for these CNVs (7). A notable example of this is the 520-kbp deletion encompassing  
86 seven genes on chromosome 16p12.1, which is associated with multiple neuropsychiatric  
87 disorders, including intellectual disability/developmental delay (ID/DD), schizophrenia, and  
88 epilepsy (8, 9). Furthermore, a large-scale study on a control population reported cognitive  
89 defects in seemingly unaffected individuals with the 16p12.1 deletion (10), suggesting that the  
90 deletion is sufficient to cause neuropsychiatric features. In contrast to other pathogenic CNVs  
91 that occur mostly *de novo*, the 16p12.1 deletion is inherited in more than 95% of individuals  
92 from a mildly affected or unaffected carrier parent (8, 9, 11). In fact, affected children with the  
93 deletion were more likely to carry another large CNV or deleterious mutation elsewhere in the  
94 genome (“second-hit”) compared to their carrier parents (8, 9), providing evidence that  
95 additional rare variants modulate the effect of the deletion. These results suggest that the 16p12.1  
96 deletion confers significant risk for disease and sensitizes the genome for a range of  
97 neuropsychiatric outcomes, while additional rare variants in the genetic background determine  
98 the ultimate phenotypic trajectory.

99         The extensive phenotypic variability and lack of chromosomal events, such as  
100 translocations and atypical deletions, have made causal gene discovery for variably-expressive  
101 CNVs such as the 16p12.1 deletion challenging. In particular, the developmental and neuronal

102 phenotypes associated with each individual 16p12.1 gene and the interaction models that explain  
103 how “second-hit” genes modulate the associated phenotypes have not been assessed. Therefore, a  
104 systematic evaluation of developmental, neuronal, and cellular defects caused by reduced  
105 expression of individual 16p12.1 genes, as well as their interactions with each other and with  
106 “second-hit” genes from patients with the deletion, would allow us to understand the functional  
107 basis of the variable phenotypes associated with the deletion. *Drosophila melanogaster* and  
108 *Xenopus laevis* serve as excellent models for systematic evaluation of developmental and tissue-  
109 specific effects of multiple genes and their genetic interactions, as they are amenable for rapid  
110 genetic manipulation and high-throughput evaluation. In fact, *Drosophila* have been classically  
111 used to study the roles of genes and genetic interactions towards developmental and neurological  
112 phenotypes (12-14). For example, Grossman and colleagues overexpressed human transgenes  
113 from chromosome 21 in flies and identified synergistic interactions between *DSCAM* and  
114 *COL6A2*, which potentially contribute to the heart defects observed in individuals with Down  
115 syndrome (15). Furthermore, functional assays using *X. laevis* have uncovered developmental  
116 defects, behaviors, and molecular mechanisms for several homologs of genes associated with  
117 neurodevelopmental disorders, such as *NLGN1* (16), *CACNA1C* (17), *GRIK2* (18), and *PTEN*  
118 (19).

119         Using *Drosophila* and *X. laevis* models, we recently found that multiple genes within the  
120 variably expressive 16p11.2 and 3q29 deletion regions individually contribute to  
121 neurodevelopmental defects (20, 21), suggesting that no single gene could be solely causative for  
122 the wide range of defects observed with deletion of an entire region. Moreover, we identified  
123 complex genetic interactions within conserved biological pathways among homologs of genes  
124 affected by these CNVs. For example, fly and *X. laevis* homologs of *NCBP2* enhanced the

125 neuronal and cellular phenotypes of each of the other homologs of 3q29 genes (21), while fly  
126 homologs of 16p11.2 genes interacted in cellular proliferation pathways in an epistatic manner to  
127 enhance or suppress phenotypes of individual homologs (20). In fact, several aspects of the  
128 interactions observed in our studies were also functionally or thematically validated in vertebrate  
129 model systems, providing further evidence for the utility of these models to study complex  
130 genetic interactions (22, 23). While our previous work showed pervasive interactions of  
131 homologs within regions associated with neurodevelopmental disease, the deletions within these  
132 regions occur primarily *de novo* (11), indicating a strong phenotypic impact associated with these  
133 CNVs. In contrast, the 16p12.1 deletion is mostly inherited and more frequently co-occurs with  
134 “second-hit” variants in affected individuals than other pathogenic CNVs (11), suggesting that  
135 interactions involving “second-hit” genes confer a higher impact towards the variable  
136 neurodevelopmental phenotypes compared to those caused by interactions among genes within  
137 the CNV region.

138       Here, using *Drosophila melanogaster* and *X. laevis* as two complementary model systems  
139 of development, we present the first systematic assessment of conserved genes within the  
140 16p12.1 deletion towards developmental, neuronal, and cellular phenotypes in functional models.  
141 We found that knockdown of each individual 16p12.1 homolog affects multiple phenotypic  
142 domains of neurodevelopment, leading to developmental delay and seizure susceptibility, brain  
143 size alterations, neuronal morphology abnormalities, and cellular proliferation defects. These  
144 defects were modulated by simultaneous knockdown of homologs of genes in established  
145 neurodevelopmental pathways and transcriptome targets, as well as homologs of genes that  
146 carried “second-hits” in affected children with the deletion, through genetic interactions and  
147 additive effects. Our results suggest a model where reduced expression of each individual gene

148 within 16p12.1 is sufficient to sensitize the genome towards distinct neurodevelopmental defects,  
149 which are then modulated by complex interactions with “second-hit” genes.  
150

## 151 **Results**

### 152 **Multiple homologs of 16p12.1 genes contribute to *Drosophila* and *X. laevis* development**

153 We identified four conserved fly homologs out of the seven human protein coding 16p12.1 genes  
154 using reciprocal BLAST and orthology prediction tools (**S1 Table**) (24). Using RNA  
155 interference (RNAi) and the *UAS-GAL4* system (25), we reduced the expression of the four fly  
156 homologs in a tissue-specific manner, and studied their individual contributions towards  
157 developmental, neuronal, and cellular defects (**Fig 1**). A complete list of the fly lines used in this  
158 study and full genotypes for all experiments are provided in **S1 File**. We authenticated the RNAi  
159 lines by confirming 40-60% expression of the four homologs using RT-qPCR (**S1 Fig**). We note  
160 that the genes are represented with fly gene names along with human counterparts at first  
161 mention in the text, and as fly genes with allele names in the figures.

162 We first assessed the global role of 16p12.1 homologs during development by decreasing  
163 their expression ubiquitously using the *da-GAL4* driver, and detected larval lethality with  
164 knockdown of *Sin* (*POLR3E*) and larval and pupal lethality with knockdown of *UQCR-C2*  
165 (*UQCRC2*) (**Fig 2A, S2 Fig**). Wing-specific *bx<sup>MS1096</sup>-GAL4* mediated knockdown led to severe  
166 phenotypes for *Sin* and severe defects and lethality for *UQCR-C2* fly models, recapitulating the  
167 observations made with ubiquitous knockdown (**Fig 2A, S2 Fig**) and suggesting a role for these  
168 homologs in signaling pathways required for early development (26-28). Next, we evaluated  
169 whether decreased expression of the homologs leads to neuronal phenotypes frequently observed  
170 in animal models of neurodevelopmental disease, including altered lifespan, susceptibility to  
171 seizures, delayed developmental timing, changes in brain size, and dendritic arbor defects (29-  
172 34). We observed early lethality in adult flies with nervous system-specific *Elav-GAL4*-mediated  
173 knockdown of *Sin* and *CG14182* (*MOSMO*) (**Fig 2B**), while extended lifespan was observed



174 with knockdown of *UQCR-C2*, as previously reported for *Hsp26*, *Hsp27* (35), and *SOD* (36).  
175 While altered mitochondrial activity has been shown to increase lifespan in *Drosophila* (37, 38),  
176 further studies are necessary to understand the mechanism underlying this phenotype observed  
177 with knockdown of *UQCR-C2*. *UQCR-C2* knockdown in the nervous system also led to  
178 significantly greater recovery time when subjected to mechanical stress during bang sensitivity  
179 assays, suggesting a higher susceptibility to developing seizures (32) (**S2 Fig**). Furthermore,  
180 evaluation of developmental transitions revealed delayed pupariation and larval lethality with  
181 knockdown of *Sin*, indicating a possible role for this gene in developmental timing, as well as  
182 partial larval lethality for *CG14182* (**Fig 2C**). Furthermore, we analyzed neuronal morphology in  
183 *Drosophila* class IV sensory neurons using the *ppk-Gal4* driver (31, 39, 40), and identified  
184 reduced complexity of dendritic arbors during development for *CG14182* (**Fig 2D**).  
185 Measurements of total area of the developing third instar larval brain led to reduced brain sizes  
186 with pan-neuronal knockdown of *CG14182* and *Sin* (**Fig 2E, S3 Fig**), which corresponded with a  
187 decreased number of cells in the brain lobe stained with anti-phosphorylated-Histone 3 (pH3), a  
188 marker for proliferating cells (**Fig 2F**). Interestingly, *Sin* knockdown also led to a reduction in  
189 the number of apoptotic cells, as indicated by staining with anti-Death-caspase-1 (Dcp-1) (**S3**  
190 **Fig**), likely reflecting its role in both proliferation and apoptotic processes (41, 42).

191 We then performed RNA-sequencing of fly heads with pan-neuronal knockdown of the  
192 16p12.1 homologs. Gene Ontology (GO) enrichment analysis of differentially expressed genes  
193 identified enrichments for multiple cellular, developmental, and neuronal processes (**S4 Fig, S2**  
194 **File**). We found that each 16p12.1 homolog disrupted unique sets of genes and biological  
195 functions, as 1,386/1,870 (74%) differentially expressed genes and 28/52 (53.8%) enriched GO  
196 biological process terms were uniquely disrupted by one homolog (**S4 Fig**). Notably, we also

197 observed this trend among the human homologs of differentially-expressed genes, with 654/994  
198 (65.8%) uniquely differentially expressed genes and 353/428 (82.5%) GO terms uniquely  
199 disrupted by the 16p12.1 homologs, suggesting that they may act within independent pathways  
200 (**S4 Fig**). For example, knockdown of *CG14182* altered the expression of fly homologs of human  
201 genes involved in synapse assembly and transmission (*NLG1*, *CEL*) as well as histone  
202 methyltransferase binding (*NOP56*, *CBX1*). Similarly, human homologs of genes differentially  
203 expressed with knockdown of *Sin* were involved in neuronal projection, neurotransmitter release  
204 (such as *CHRNA7*, *KCNAB2*, and multiple solute carrier transport family genes, including  
205 *SLC6A1*), and GABA pathways (such as *ADCY2*, *ADCY4*, and *ADCY7*), as well as in the  
206 development of several non-neuronal organ systems, including cardiac, kidney, lung, and  
207 muscle, further indicating the importance of *Sin* towards global development.

208         Next, we examined developmental phenotypes associated with decreased dosage of  
209 homologs of 16p12.1 genes in *X. laevis*, a complementary vertebrate model system (**Fig 1** and  
210 **2G**). We injected homolog-specific morpholinos at two- or four-cell stage embryos to reduce the  
211 expression of each homolog to approximately 50% (partial knockdown), and further reduced  
212 expression with higher morpholino concentrations (stronger knockdown) to increase our  
213 sensitivity to detect more specific phenotypes (**S1 Fig**, see **Methods**). Reduced expression of  
214 *mosmo* and *polr3e* led to severe craniofacial defects in stage 42 tadpoles, as measured by specific  
215 facial landmarks, while milder defects were observed for *cdr2* (**Fig 2H, S5 Fig**). This suggests a  
216 role for these homologs in key developmental processes involved in craniofacial morphogenesis,  
217 such as neural crest cell formation and migration (43-48), and could potentially explain the  
218 craniofacial changes observed in more than 50% of individuals with the 16p12.1 deletion (9). We  
219 next examined axon outgrowth phenotypes in neural tube explants from stage 20-22 injected *X*.

220 *laevis* embryos, and found that stronger knockdown of *mosmo* (20 ng morpholino) led to a  
221 significant reduction in axon length (**Fig 2I, S5 Fig**), suggesting a potential role for the homolog  
222 in cytoskeletal signaling processes involved in axon outgrowth (49). Furthermore, stronger  
223 knockdown of *mosmo* (20 ng morpholino) and *polr3e* (20 ng morpholino) resulted in decreased  
224 forebrain and midbrain area (**Fig 2J, S5 Fig**), in concordance with the brain size defects we  
225 observed in *Drosophila* models. Interestingly, partial knockdown of *mosmo* (12 ng morpholino)  
226 also led to a severe reduction in forebrain and midbrain area (**S5 Fig**). Western blot analysis for  
227 whole embryo lysates using anti-pH3 antibody as a marker for cellular proliferation showed  
228 decreased proliferation with knockdown of *polr3e*, while knockdown of *mosmo* did not lead to  
229 any significant changes (**S6 Fig**). Overall, these results suggest that homologs of 16p12.1 genes  
230 individually contribute to multiple developmental defects and affect distinct developmental,  
231 neuronal, and cellular processes in *Drosophila* and *X. laevis*.

232

### 233 **Additive effects and genetic interactions among 16p12.1 homologs mediate** 234 **neurodevelopmental defects**

235 Our previous studies identified several potential models for how genes within CNVs interact  
236 with each other to influence neurodevelopmental phenotypes (20, 21, 50). As multiple homologs  
237 of 16p12.1 genes contribute towards developmental, neuronal, and cellular phenotypes, we used  
238 the sensitive fly eye system to assess for genetic interactions among the 16p12.1 fly homologs.  
239 The *Drosophila* fly eye has been widely used to identify genetic interactions that disrupt  
240 ommatidial organization during development (51), and modifier genes for homologs of several  
241 human diseases, including Spinocerebellar ataxia type 1 (52), Huntington's disease (52), and  
242 Fragile X syndrome (53), have been studied in flies. We first assessed whether eye-specific

243 *GMR-GAL4* knockdown of individual homologs led to eye phenotypes, and evaluated the  
244 severity of eye roughness using *Flynotyper*, a tool that quantifies the levels of ommatidial  
245 disorderliness in the adult fly eye (54). We observed that knockdown of *Sin* led to a subtle  
246 disruption of ommatidial organization compared with the control, while no such phenotypes  
247 were observed with knockdown of the other homologs (**S7 Fig**). Further reductions in expression  
248 of the 16p12.1 homologs using *GMR-GAL4* and overexpression of *Dicer2* led to more severe eye  
249 phenotypes for *CG14182* and *Sin* (**S7 Fig**). As *GMR-GAL4*-mediated knockdown of the 16p12.1  
250 homologs only exhibited modest eye phenotypes, we next took advantage of *Flynotyper* scores  
251 as a quantitative trait with high sensitivity and a wide dynamic range to assess for genetic  
252 interactions among the 16p12.1 homologs. We therefore generated *GMR-GAL4* eye-specific  
253 recombinant lines for each homolog and crossed them with multiple RNAi lines for other  
254 16p12.1 homologs (see **Methods, S1 File**), to test a total of 30 two-hit crosses for 12 pairwise  
255 gene interactions (**Fig 1 and 3A, S8 Fig**). We observed significant changes in eye severity for  
256 four pairwise combinations of knockdowns compared with single hit recombinant lines crossed  
257 with controls, which were validated with multiple RNAi lines (**S3 File**). For example, we  
258 observed that simultaneous knockdown of *UQCR-C2* with *Sin* or *CG14182* led to an increase in  
259 eye phenotype compared to knockdown of *UQCR-C2* crossed with control (**Fig 3B and 3C**).  
260 Similarly, decreased expression of *Sin* led to an enhancement of the *CG14182* eye phenotype.

261 In order to quantitatively assess whether the phenotypes observed with pairwise  
262 knockdowns could be attributed to either genetic interactions or expected additive effects, we  
263 applied a “multiplicative” model to the *Flynotyper* scores of pairwise knockdowns. The  
264 multiplicative model estimates the expected combined effect (i.e., no interaction) of two gene  
265 mutations as the product of the phenotypes observed with individual gene mutations (**Fig 3D, S9**

266 **Fig**), and identifies any deviation of the observed phenotypes from the expected values as  
267 positive (ameliorating the phenotype) or negative/synergistic (aggravating the phenotype)  
268 interactions. This strategy has been widely applied to identify fitness-based genetic interactions  
269 (55, 56), and more recently, to assess for interactions contributing to non-fitness-related  
270 quantitative phenotypes, such as cell count, nuclear area (57), and protein folding in the  
271 endoplasmic reticulum (58). After applying the multiplicative model to our pairwise interaction  
272 data, we identified five pairwise combinations of 16p12.1 homologs that were validated using  
273 multiple RNAi lines (**S2 Table**). Two pairwise combinations corresponded with no interactions  
274 or additive effects, while the remaining three were positive genetic interactions, with an observed  
275 phenotype milder than expected (**S3 File**). Only one out of the four pairwise knockdowns that  
276 resulted in significant changes in eye severity compared with single hit recombinant lines  
277 crossed with control (**S3 File**) corresponded with a genetic interaction, while the rest were not  
278 validated across multiple fly lines tested. To contextualize these observations, we compared the  
279 strength of genetic interactions among the 16p12.1 homologs to those of homologs of genes  
280 affected by the autism-associated 16p11.2 deletion, a region with reported pervasive genetic  
281 interactions (20). We quantified the magnitude of genetic interactions using “interaction scores”,  
282 defined as the  $\log_2$  ratio between the observed and expected phenotypic values from the  
283 multiplicative model (see **Methods**), and found significantly lower interaction scores for the  
284 16p12.1 homologs compared to the 16p11.2 homologs (**S4 File**).

285 We further investigated the effects of the combined knockdown of homologs of *MOSMO*  
286 and *POLR3E*, genes that individually contributed to multiple defects in both fly and *X. laevis*  
287 models, towards *X. laevis* development (**Fig 1** and **3E**). Pairwise interactions in *X. laevis* models  
288 were tested using partial knockdown of the homologs to avoid potential lethality with stronger

289 knockdown. Partial pairwise knockdown of *polr3e* (10 ng morpholino) and *mosmo* (12 ng  
290 morpholino) showed significantly reduced forebrain and midbrain area when compared to  
291 knockdown of *polr3e* alone (**Fig 3F**), but not when compared to knockdown of *mosmo* alone.  
292 Similarly, we assessed whether *mosmo* and *polr3e* interact to modulate cellular proliferation  
293 processes during *X. laevis* development and did not observe any changes in anti-pH3 signals with  
294 combined knockdown of *polr3e* and *mosmo* compared with knockdown of *polr3e* alone (**Fig 3G,**  
295 **S6 Fig**). Overall, our analysis in *Drosophila* and *X. laevis* suggest that 16p12.1 homologs  
296 contribute towards neurodevelopmental phenotypes through both genetic interactions and  
297 additive effects.

298

### 299 **Homologs of 16p12.1 genes interact with genes in conserved neurodevelopmental pathways**

300 We recently identified genetic interactions between fly homologs of CNV genes and conserved  
301 genes in neurodevelopmental pathways, providing functional evidence that phenotypes of CNV  
302 genes are modulated by key neurodevelopmental genes (20, 21). As our functional analyses  
303 showed that knockdown of each 16p12.1 homolog resulted in multiple neuronal and  
304 developmental phenotypes, we hypothesized that genes involved in conserved  
305 neurodevelopmental pathways could modulate phenotypes due to knockdown of 16p12.1  
306 homologs through genetic interactions. We therefore performed 255 crosses to test 116 pairwise  
307 gene combinations between eye-specific recombinant lines for each of the four 16p12.1  
308 homologs and 13 homologs of known neurodevelopmental genes and 39 homologs of  
309 transcriptional targets (**Fig 4A, S10 Fig, S2 Table, S3 Table**). As validation, we used multiple  
310 RNAi, mutant or overexpression lines when available (**Fig 1**). Details of the number of  
311 homologs, fly lines, and crosses used for all interaction experiments are provided in **S2 Table**.

312 *First*, we screened for 55 combinations between homologs of 16p12.1 genes and 13 homologs of  
313 human genes in established developmental pathways, such as synapse function  
314 (*Prosap/SHANK3*), cell division (*Pten/PTEN*), and chromatin modulation (*kis/CHD8*), as well as  
315 genes functionally related to 16p12.1 homologs (54, 59-61). Using *Flyntyper* to quantify adult  
316 eye defects and the multiplicative model to identify genetic interactions, we identified  
317 interactions specific to an individual 16p12.1 homolog or those involving multiple homologs  
318 (**S11-S16 Fig, S3 File**). For example, *CG10465 (KCTD13)* negatively interacted with *UQCR-C2*  
319 and *CG14182*, leading to significantly more severe phenotypes than expected using the  
320 multiplicative model (**Fig 4B**). Similarly, simultaneous knockdown of *Sin* with *kis* led to an  
321 exaggerated eye phenotype, suggesting negative interactions between the genes (**Fig 4B**).  
322 Overall, we confirmed 22 interactions out of the 55 pairwise combinations (40%) tested,  
323 including both positive (12/55) and negative (10/55) effects (**Fig 4C-D, S17 Fig, S2 Table**).  
324 *Next*, to correlate 16p12.1 homologs to developmental functions and pathways (**S10 Fig, S3**  
325 **Table**), we screened for interactions of the homologs with 25 dysregulated fly genes selected  
326 from our transcriptome studies as well as 14 genes within enriched Gene Ontology categories,  
327 such as nervous system development and function (*Dscam1, Asp, mGluR, NaCP60E*), protein  
328 folding (*Hsp23, Hsp26, Hsp70Ab*), and muscle contraction (*Actn, ck*). We identified interactions  
329 for 42 out of 61 tested pairs (68.8%, **S2 Table**), validated using additional lines when available  
330 (**S3 File**). For example, knockdown of *Gat (SLC6A1)*, *Dscam4 (DSCAM)*, *Nipped-A (TRRAP)*,  
331 and *aurB (AURKB)* each modified the eye phenotype due to knockdown of *Sin* through positive  
332 or negative genetic interactions (**Fig 4C, S13 Fig, S16 Fig, S3 File**). Furthermore, the protein-  
333 folding gene *Hsp26 (CRYAA)* was differentially expressed with knockdown of *Cen*, and its  
334 knockdown enhanced the phenotype of *Cen* through a negative interaction (**Fig 4C, S12 Fig, S3**

335 **File**). Overall, we identified 64 pairwise interactions between the 16p12.1 homologs and genes  
336 from established neuronal functions and transcriptome targets (**Fig 4C-D, S2 Table**), further  
337 suggesting an involvement of these homologs in multiple neurodevelopmental pathways.

338

### 339 **Homologs of patient-specific “second-hit” genes modulate phenotypes of 16p12.1 homologs**

340 We recently found that an increased burden of rare variants (or “second-hits”) outside of disease-  
341 associated CNVs, such as 16p11.2 deletion, 15q13.3 deletion, and 16p12.1 deletion, contributed  
342 to variability of cognitive and developmental phenotypes among affected children with these  
343 CNVs (8, 9, 11). In fact, we found that severely affected children with the 16p12.1 deletion had  
344 additional loss-of-function or severe missense variants within functionally intolerant genes  
345 compared to their mildly affected carrier parents (8, 9, 11). We hypothesized that homologs of  
346 genes carrying patient-specific “second-hits” modulate the effects of individual 16p12.1  
347 homologs not only additively but also through genetic interactions (**S10 Fig, S3 Table**). To test  
348 this, we performed 227 crosses to study 96 pairwise interactions between eye-specific  
349 recombinant lines for each of the four 16p12.1 homologs and 46 RNAi or mutant lines for 24  
350 homologs of patient-specific “second-hit” genes identified in 15 families with the 16p12.1  
351 deletion (**Fig 1, S18 Fig, S2-S4 Tables**) (9). Out of the 96 combinations tested, we identified 32  
352 pairwise knockdowns that modulated the phenotype of a 16p12.1 homolog, confirmed with  
353 additional lines when available, for 11 out of 15 families carrying “second-hit” genes (**Fig 5A-C,**  
354 **S2-S4 Tables**). In fact, the phenotypic effects of 16 out of 32 combinations were attributed to  
355 genetic interactions (**Fig 4D, S3 File**). Interestingly, we observed that different “second-hit”  
356 homologs showed distinct patterns of interactions with homologs of 16p12.1 genes (**Fig 5B, S3**  
357 **File**). For example, the affected child in family GL\_11 carried “second-hit” pathogenic



358 mutations in *NRXN1* and *CEP135* (**Fig 5A**). Knockdown of the fly homolog *Nrx-1* enhanced the  
359 eye phenotype caused by knockdown of *Sin* and *UQCR-C2*, while simultaneous knockdown of  
360 *Cep135* with *UQCR-C2* led to lower phenotypic score compared to knockdown of *UQCR-C2*  
361 alone (**Fig 5B**). While the two-hit phenotypes were not significantly different from the expected  
362 combined effects of the individual genes in these cases (**S3 File**), we observed genetic  
363 interactions between *Nrx-1* and *CG14182*, and *Cep135* and *Sin* or *Cen*, suggesting potential  
364 functional connections between these genes (**Fig 5D**). Interestingly, for 11/96 combinations  
365 tested with the multiplicative model, we found that the phenotype of the pairwise knockdown  
366 was more severe compared to the phenotype observed for the knockdown of an individual  
367 16p12.1 homolog, but significantly less severe than the expected effects, suggesting potential  
368 buffering against deleterious additive effects (62, 63) (**Fig 4C, Fig 5D, S3 File**). In another  
369 example, the affected child in family GL\_01 carried inherited “second-hit” variants in *LAMC3*  
370 and *DMD*, as well as a *de novo* loss-of-function mutation in the intellectual disability-associated  
371 and chromatin regulator gene *SETD5* (64) (**S18 Fig**). Knockdown of *Lanb2*, homolog of *LAMC3*,  
372 enhanced the phenotype caused by knockdown of *UQCR-C2*, although they positively interacted  
373 towards a milder phenotype than expected (**S3 File**). Furthermore, *upSET*, homolog of *SETD5*,  
374 led to enhancements of the phenotypes caused by knockdown of *Sin* and *CG14182* (**S3 File**).  
375 Interestingly, while the phenotype caused by simultaneous knockdown of *Sin* and *upSET* was not  
376 different from expected using the multiplicative model, *upSET* synergistically interacted with  
377 *CG14182*, leading to an enhanced eye phenotype with pairwise knockdown (**Fig 6A**). To assess  
378 the cellular changes affected by this interaction during development, we tested for alterations in  
379 apoptosis and proliferation in the third instar larval eye discs, and found that simultaneous  
380 knockdown of *CG14182* and *upSET* led to an increased number of cells undergoing proliferation

381 and apoptosis compared to knockdown of *CGI4182* alone (**Fig 6B**). Interestingly, we also  
382 identified interactions between *CGI4182* and other chromatin modifier genes, including *Nipped-*  
383 *A*, a transcriptional target of *Sin*, and *Osa*, homolog of the “second-hit” gene *ARID1B*, identified  
384 in family GL\_13 (**S16 Fig, S3 File**). These interactions also modulated cellular proliferation and  
385 apoptosis processes in the developing eye discs observed with knockdown of *CGI4182* (**S19**  
386 **Fig**).

387 We further evaluated whether interactions between the fly homologs of *POLR3E* and  
388 *MOSMO* with *SETD5* were also conserved during vertebrate development, and studied brain and  
389 axon outgrowth phenotypes of homologs of these genes in *X. laevis* (**Fig 1**). We observed that  
390 simultaneous knockdown of *polr3e* and *setd5* led to smaller forebrain and midbrain areas  
391 compared with *polr3e* knockdown alone (**S20 Fig**). Similarly, simultaneous knockdown of  
392 *mosmo* and *setd5* led to a further reduction in midbrain area than that observed with knockdown  
393 of *mosmo* alone (**Fig 6C**). Furthermore, analysis of axon outgrowth in developing *X. laevis*  
394 embryos showed that simultaneous knockdown of *mosmo* and *setd5* led to significantly reduced  
395 axon length compared to the individual knockdowns of either *mosmo* or *setd5*, while no changes  
396 were observed with simultaneous knockdown of *polr3e* and *setd5* (**Fig 6D, S20 Fig**). In fact, the  
397 axon outgrowth defect observed with simultaneous knockdown of *mosmo* and *setd5* was not  
398 observed with partial knockdown of either individual homolog. This result suggests a genetic  
399 interaction between *mosmo* and *setd5* during vertebrate nervous system development. Overall,  
400 our results show that interactions with “second-hit” genes can modulate neurodevelopmental and  
401 cellular phenotypes associated with homologs of 16p12.1 genes.

402

## 403 Discussion

404 We previously described multiple models for how genes within CNVs contribute towards  
405 neurodevelopmental phenotypes (20, 21, 50). Here, we analyzed neurodevelopmental defects and  
406 cellular and molecular mechanisms due to individual and pairwise knockdown of conserved  
407 16p12.1 homologs in *Drosophila* and *X. laevis*, and evaluated how these defects are modulated  
408 by homologs of “second-hit” genes. Our results provide multiple hypotheses for how genes  
409 within the deletion contribute to neurodevelopmental phenotypes. *First*, in line with our previous  
410 findings for homologs of genes within CNV regions (20, 21), our results show that no single  
411 homolog within the 16p12.1 region is solely responsible for the observed neurodevelopmental  
412 phenotypes. In fact, we observed a global developmental role for multiple 16p12.1 homologs, as  
413 well as specific roles of each homolog towards craniofacial and brain development (**S5 Table**).  
414 This was further confirmed by interactions of 16p12.1 homologs with genes in conserved  
415 neurodevelopmental pathways. Our findings are in accordance with the core biological functions  
416 described for some of these genes. *For example*, *POLR3E* encodes a cofactor of the RNA  
417 polymerase III, which is involved in the transcription of small RNA, 5S ribosomal RNA and  
418 tRNA (65), while *MOSMO* is a negative regulator of the hedgehog signaling pathway (66).  
419 *Second*, knockdown of individual homologs sensitized both model organisms towards specific  
420 phenotypes. For example, knockdown of homologs of *MOSMO* led to neuronal morphology  
421 defects and knockdown of homologs of *POLR3E* led to brain size phenotypes that correlated  
422 with cellular proliferation defects in both model systems, while knockdown of *UQCR-C2* led to  
423 seizure susceptibility in flies. *Third*, we found that the 16p12.1 homologs were less likely to  
424 interact with each other (3 interactions out of 12 pairs tested) compared to their interactions with  
425 downstream transcriptome targets (42 interactions out of 61 pairs tested, Fisher’s exact test,

426  $p=0.0077$ ). These results suggest reduced functional overlap among the 16p12.1 homologs, an  
427 observation supported by the distinct sets of biological functions enriched among the  
428 differentially expressed genes obtained with knockdown of each individual homolog (**S4 Fig**).  
429 Beyond the four conserved homologs evaluated in this study, little functional information is  
430 available on the other genes in the region, including *VWA3A* and *PDZD9* as well as non-protein  
431 coding genes. Results from mouse models of *EEF2K*, which encodes a kinase associated with  
432 protein synthesis elongation, have postulated associations of this gene with synaptic plasticity  
433 (67), learning and memory (68), atherosclerosis-mediated cardiovascular disease (69), and  
434 depression (70). Although *EEF2K* could function in concert with the tested 16p12.1 genes to  
435 contribute towards neurodevelopmental features, it showed low connectivity (29<sup>th</sup> percentile) to  
436 other 16p12.1 genes in a human brain-specific interaction network compared to the pairwise  
437 connectivity of all genes in the network (71, 72) (**S5 File**). *VWA3A* showed even lower  
438 connectivity (5<sup>th</sup> percentile) to other 16p12.1 genes compared to all gene pairs, suggesting that  
439 16p12.1 genes with no fly homologs are likely to show reduced network connectivity in the  
440 human brain. Further functional analyses that includes all protein-coding and non-coding genes  
441 are necessary for a comprehensive understanding of the consequences of the entire deleted  
442 region, as these genes may also contribute towards the pathogenicity of 16p12.1 deletion.

443         We recently showed that additional variants or “second-hits” modulate the manifestation  
444 of developmental and cognitive phenotypes associated with disease-causing variants, including  
445 intelligence quotient and head circumference phenotypes (8, 9, 11). Using the 16p12.1 deletion  
446 as a paradigm for complex genetics, we examined how homologs of genes carrying “second-hit”  
447 variants modulate the phenotypes caused by decreased expression of individual CNV homologs.  
448 For example, homologs of *ARID1B*, *CEP135* and *CACNA1A* suppressed the eye phenotypes and

449 interacted with one or more 16p12.1 homologs. Furthermore, we identified a negative interaction  
450 between homologs of *MOSMO* and *SETD5*, which led to novel neurodevelopmental phenotypes  
451 in both *Drosophila* and *X. laevis* compared with knockdown of either individual homolog.  
452 Interestingly, mouse embryonic stem cells lacking *Setd5* exhibited dysregulation of genes  
453 involved in hedgehog signaling (73), a key pathway recently associated with *MOSMO* function  
454 (66). Moreover, we observed that *MOSMO* and *SETD5* are highly connected to each other in a  
455 human brain-specific interaction network compared to all genes in the genome (top 84<sup>th</sup>  
456 percentile compared to all genetic interactions with *MOSMO*), suggesting that the human genes  
457 may also be functionally related (71, 72). We further observed interactions between *CG14182*  
458 and other genes with chromatin regulating function, such as *Nipped-A* (*TRRAP*) and *osa*  
459 (*ARID1B*) (**S16 Fig**). Based on these observations, we propose that while genes carrying  
460 “second-hit” variants may additively contribute towards more severe phenotypes, they may also  
461 interact towards developmental phenotypes, conferring high impact towards variable  
462 neurodevelopmental defects associated with the 16p12.1 deletion. The ultimate nature of these  
463 interactions depends on the role of the individual CNV genes towards specific phenotypes, as  
464 well as the molecular complexity associated with each phenotypic domain (50).

465         The high inheritance rate of the 16p12.1 deletion (8, 9) suggests that while it confers risk  
466 for several phenotypes, the CNV can be transmitted through multiple generations until additional  
467 variants accumulate and cumulatively surpass the threshold for severe disease (7). In contrast,  
468 other CNVs associated with neurodevelopmental disease, such as the autism-associated 16p11.2  
469 deletion and the 17p11.2 deletion that causes Smith-Magenis syndrome, occur mostly *de novo*  
470 and are less likely to co-occur with another “second-hit”, suggesting a higher pathogenicity on  
471 their own (11). For example, the 16p11.2 deletion occurs *de novo* in approximately 60% of the

472 cases, and only 8% of the affected children carry another rare large CNV, in contrast to 25% of  
473 severely affected children with 16p12.1 deletion that carry a “second-hit” large CNV (11). When  
474 we compared experimental results from 16p12.1 homologs with those for fly homologs of  
475 16p11.2 genes (20), we found evidence that the differential pathogenicity of the CNVs could be  
476 explained by differential connectivity and combinatorial effects of genes within each region (**Fig**  
477 **7A**) (74). For example, we previously found that 24 out of the 52 tested pairwise knockdowns of  
478 16p11.2 homologs led to enhancement or suppression of phenotypes, significantly modifying the  
479 effect of the individual genes (20). In contrast, only four out of twelve tested combinations  
480 between 16p12.1 homologs led to a slight change in phenotypic severity, which in aggregate  
481 showed lower phenotypic scores than those observed for pairwise knockdown of 16p11.2  
482 homologs (**Fig 7B** and **S21 Fig**). In fact, using a multiplicative model, we found that the  
483 magnitude of interactions between homologs of 16p11.2 genes was stronger than that observed  
484 between 16p12.1 homologs (**Fig 7C**). Moreover, transcriptome analyses showed a higher overlap  
485 of differentially expressed genes among 16p11.2 homologs compared to 16p12.1 homologs,  
486 further suggesting a higher functional relatedness among the 16p11.2 genes (**Fig 7D**). We  
487 similarly compared the connectivity of genes within both CNV regions in a human brain-specific  
488 interaction network (71, 72), and found that 16p11.2 genes were more strongly connected to each  
489 other than were 16p12.1 genes, and were also more strongly connected to each other than with  
490 other genes in the genome (**Fig 7E and 7F, S21 Fig**). Interestingly, genes connecting pairs of  
491 16p11.2 genes were enriched for genes intolerant to functional variation (**Fig 7E and 7G**), such  
492 as *ASH1L*, a histone methyltransferase activator and autism candidate gene (75), and *CAMK2B*, a  
493 protein kinase gene causative for intellectual disability (76). In contrast, connector genes unique  
494 to 16p12.1 genes were not associated with neurodevelopmental disease or enriched for genes

495 intolerant to variation (**S5 File**). This suggests that the 16p11.2 deletion disrupts a tight network  
496 of key genes in the brain, including other neurodevelopmental genes and genes with disease  
497 relevance (77, 78). Overall, we propose that 16p12.1 genes contribute towards multiple  
498 neurodevelopmental phenotypes through genetic interactions and additive effects with “second-  
499 hit” genes and exhibit less functional connectivity compared with 16p11.2 genes, leading to a  
500 high transmissibility of the deletion and higher impact of additional “second-hit” variants  
501 towards neurodevelopmental phenotypes.

502 Our study provides the first systematic analysis of individual and pair-wise contributions  
503 of 16p12.1 homologs towards basic neurodevelopmental phenotypes and cellular and molecular  
504 mechanisms, and identifies a key role of genetic interactions with “second-hit” homologs  
505 towards variable developmental phenotypes. Our work does not intend to recapitulate human  
506 disease, but rather to highlight the basic cellular roles of individual conserved genes and their  
507 interactions towards neurodevelopmental phenotypes. As such, these findings should be further  
508 examined in higher-order model systems, including mouse and human cellular models. Our  
509 functional analyses suggest a model where 16p12.1 genes sensitize towards different domains of  
510 neurodevelopment, but the ultimate phenotypic manifestation would depend on complex  
511 interactions with genes that carry “second-hit” variants in the genetic background. Our results  
512 highlight the importance of a thorough functional characterization of both individual CNV genes  
513 and their interactions with genes carrying “second-hit” variants towards disease-associated  
514 phenotypes.

515

516

517

518

## 519 **Materials and Methods**

### 520 **Ethics statement**

521 All *X. laevis* experiments were approved by the Boston College Institutional Animal Care and  
522 Use Committee (Protocol #2016–012), and were performed according to national regulatory  
523 standards.

524

### 525 ***Drosophila* stocks and genetics**

526 Using *Ensembl* database (79), NCBI Protein-Protein BLAST tool (80), and DRSC Integrative  
527 Ortholog Prediction Tool (DIOPT) (24), we identified four homologs out of the seven genes  
528 within the 16p12.1 deletion region in *Drosophila melanogaster* (**S1 Table**). No fly homologs  
529 were present for three genes, including *VWA3A*, *PDZD9* and *EEF2K*. Similar strategies were  
530 used to identify fly homologs of conserved neurodevelopmental genes and genes carrying  
531 “second-hits” in children with the 16p12.1 deletion. Fly Atlas Anatomy microarray expression  
532 data from FlyBase confirmed the expression of each 16p12.1 homolog in the nervous system  
533 during *Drosophila* development (**S1 Table**) (81), and expression data from Xenbase (82)  
534 confirmed the expression of the homologs in *X. laevis* brain.

535 Multiple RNAi lines were used to test neurodevelopmental defects of 16p12.1 homologs  
536 (S1 File). RNAi, mutant, or overexpression lines for fly homologs were obtained from the  
537 Vienna Stock Resource Center (VDRC), Bloomington *Drosophila* Stock Center (BDSC) (NIH  
538 P40OD018537), or Kyoto Stock Center (S1 File). The following lines used were generated in  
539 various research labs: *Drice*<sup>17-1</sup> and *Drice*<sup>17-2</sup> from Bergmann lab (83), *GluRIIB*<sup>Overexp EGFP</sup> from  
540 Sigrist lab (84), *Hsp26*<sup>Overexp Hsp26</sup> from Benzer lab (35), and *Hsp70Ab*<sup>Overexp Hsp70-9.1</sup> and  
541 *Hsp70Ab*<sup>Overexp Hsp70-4.3</sup> from Robertson lab (85). Tissue-specific knockdown of homologs of



542 16p12.1 genes was achieved using the *UAS-GAL4* system (25), with specific *GAL4* lines  
543 including *w<sup>1118</sup>;dCad-GFP*, *GMR-GAL4/CyO* (Zhi-Chun Lai, Penn State University),  
544 *w<sup>1118</sup>;GMR-GAL4; UAS-Dicer2* (Claire Thomas, Penn State University), *w<sup>1118</sup>,mcd8-GFP*, *Elav-*  
545 *GAL4/Fm7c;; UAS-Dicer2* (Scott Selleck, Penn State University), *w<sup>1118</sup>,Elav-GAL4* (Mike  
546 Grotewiel, VCU), *w<sup>1118</sup>;;Elav-GAL4,UAS-Dicer2* (Scott Selleck, Penn State University),  
547 *w<sup>1118</sup>;da- GAL4* (Scott Selleck, Penn State University), *w<sup>1118</sup>,bx<sup>MS1096</sup>-GAL4;; UAS-Dicer2* (Zhi-  
548 Chun Lai, Penn State University), and *UAS-Dicer2; ppk-GAL4, UAS-mCD8-GFP* (Melissa  
549 Rolls, Penn State University). A list of full genotypes for all fly lines and crosses tested in this  
550 study is provided in **S1 File**. Fly crosses were reared on a cornmeal-sucrose-dextrose-yeast  
551 medium at room temperature (RT), 25°C or 30°C. For all experiments, RNAi lines were  
552 compared to a control with the same genetic background to account for background-specific  
553 effects (**S1 File**). Three different controls were used: *w<sup>1118</sup>* from VDRC (GD stock # 60000), in  
554 which inverted repeats are inserted by P-element insertion; *y,w<sup>1118</sup>* from VDRC (KK stock #  
555 60100), where inverted repeats are inserted by site-specific recombination; and *{y[1] v[1];*  
556 *P{y[+t7.7]=CaryP}attP2* from BDSC (TRiP stock # 36303).

557

### 558 **RT-quantitative PCR for *Drosophila* RNAi knockdown of 16p12.1 homologs**

559 Decreased expression of homologs of 16p12.1 genes in the nervous system was confirmed using  
560 reverse transcription quantitative PCR (RT-qPCR) for individual *Drosophila* RNAi lines.

561 Decreased expression of the genes was achieved using *Elav-GAL4;;UAS-Dicer2* lines, reared at  
562 25°C. As nervous system-specific knockdown of *Sin* with *Elav-GAL4;;UAS-Dicer2* caused  
563 developmental lethality in all three RNAi lines tested (*Sin<sup>GD7027</sup>*, *Sin<sup>KK101936</sup>*, *Sin<sup>HMC03807</sup>*), we  
564 confirmed knockdown of *Sin* using *Elav-GAL4* without overexpression of *Dicer2* and reared at

565 RT. We note that all experiments with nervous system-specific knockdown of *Sin* were  
566 performed under these conditions. Briefly, three biological replicates, each containing 35-40  
567 female heads, were collected after being separated by repeated freezing in liquid nitrogen and  
568 vortex cycles. Total RNA was extracted from *Drosophila* heads using TRIzol (Invitrogen,  
569 Carlsbad, CA, USA), and cDNA was generated using qScript cDNA synthesis kit (Quantabio,  
570 Beverly, MA, USA). Quantitative RT-PCR was performed in an Applied Biosystems Fast 7500  
571 system using SYBR Green PCR master mix (Quantabio), with *rp49* as the reference gene.  
572 Primers were designed using NCBI Primer-BLAST (86), with primer pairs separated by an  
573 intron in the corresponding genomic DNA, if possible. **S6 Table** details the primers used to  
574 quantify the level of expression of 16p12.1 homologs. The delta-delta Ct method was used to  
575 calculate the percentage of expression compared to the control (87), and statistical significance  
576 compared to the control was determined using t-tests.

577

### 578 **Eye and wing imaging**

579 Eye-specific knockdown of the 16p12.1 homologs was achieved using *GMR-GAL4* driver at  
580 30°C. Female progeny were collected on day 2-3 and imaged using an Olympus BX53  
581 compound microscope with LMPLan N 20X air objective and a DP73 c-mount camera at 0.5X  
582 magnification, with a z-step size of 12.1µm (Olympus Corporation, Tokyo, Japan). Individual  
583 image slices were captured using the CellSens Dimension software (Olympus Corporation,  
584 Tokyo, Japan), and were stacked into their maximum projection using Zerene Stacker software  
585 (Zerene Systems, Richland, WA, USA). Wing phenotypes were assessed in day 2-5 female  
586 progeny from *bx<sup>MS1096</sup>-GAL4* lines crossed to the RNAi lines at 25°C. Adult wings were imaged  
587 using a Zeiss Discovery V20 stereoscope (Zeiss, Thornwood, NY, USA) and a ProgRes Speed

588 XT Core 3 camera (Jenoptik AG, Jena, Germany) with a 40X objective. Adult wing images were  
589 captured using ProgRes CapturePro v.2.8.8 software. We characterized qualitative phenotypes  
590 for between 10-20 wing images, including curly, wrinkled, shriveled, dusky or vein defects, and  
591 10-30 eye images were assessed for rough, glazed, eye size, and necrotic patches defects.  
592 Quantitative assessment of rough adult eye phenotypes was performed using a software called  
593 *Flynotyper* (20, 54), which calculates a phenotypic score for each eye image by integrating the  
594 distances and angles between neighboring ommatidia. The phenotypic scores generated by  
595 *Flynotyper* were compared between RNAi lines and their respective controls using one-tailed  
596 Mann-Whitney tests, with Benjamini-Hochberg correction for multiple tests.

597

### 598 **Lifespan Measurement**

599 Lifespan assessment of homologs of 16p12.1 genes was performed as previously reported (88).  
600 Briefly, fly crosses were set up at 25°C with *Elav-GAL4;;UAS-Dicer2* for each of the fly  
601 homologs, or *Elav-GAL4* at RT for *Sin<sup>GD7027</sup>*. In all cases, the newly emerged progeny were  
602 collected every day for five consecutive days, and the birth date was recorded. F1 flies were  
603 allowed to mate for 24 hours, and were separated under CO<sub>2</sub> into at least four vials, each  
604 containing 20 females. Vials were transferred every 2-3 days, and the age and number of living  
605 flies were registered. One-way repeated measures ANOVA with post-hoc pairwise t-tests were  
606 performed to identify changes in lifespan for the individual 16p12.1 homologs.

607

### 608 **Bang-sensitive assay**

609 Sensitivity to mechanical stress was assessed in females with decreased expression of 16p12.1  
610 homologs in the nervous system, using *Elav-GAL4;;UAS-Dicer2* and reared at 25°C. *Sin* was

611 excluded from the analysis, as adult flies with *Elav-GALA* knockdown of the gene exhibited  
612 severe motor defects. Ten female flies from the progeny were collected on day 0-1 for ten  
613 consecutive days, and experiments were performed on day 2-3. Flies were individually separated  
614 under CO<sub>2</sub> 24 hours before the experiments, collected in culture vials containing food, and  
615 transferred to another empty culture vial the day of the experiment. Identification of bang-  
616 sensitive phenotypes was performed as previously reported (89). Each vial was vortexed at  
617 maximum speed (Fischer Scientific) for 15 seconds, and the time for each fly to recover from  
618 paralysis was registered. Differences in bang-sensitivity compared with controls were identified  
619 using two-tailed Mann-Whitney tests.

620

#### 621 **Assessment of delay in developmental timing**

622 Pupariation time was assessed in third instar larvae obtained from crosses between RNAi lines  
623 and *w<sup>1118</sup>; ;Elav-GALA, UAS-Dicer2* or *w<sup>1118</sup>, Elav-GAL4* flies. Developmentally-synced larvae  
624 were obtained from apple juice plates with yeast paste, and were reared for 24 hours. Thirty  
625 newly emerged first instar larvae were transferred to culture vials, for a total of four to ten vials  
626 per RNAi line tested. The number of larvae transitioning to pupae were counted every 24 hours.  
627 Significant differences in pupariation timing compared with the control across the duration of the  
628 experiment were identified with one-way repeated measures ANOVA and post-hoc pairwise t-  
629 tests.

630

#### 631 **Dendritic arborization experiments**

632 Class IV sensory neuron-specific knockdown was achieved by crossing the RNAi lines to *UAS-*  
633 *Dicer2; ppk-GAL4* driver at 25°C in apple juice plates. First instar larvae were collected and

634 transferred to cornmeal-based food plates for 48 hours. Z-stack images of the dorsal side of third  
635 instar larvae were obtained using a Zeiss LSM 800 (Zeiss, Thornwood, NY, USA) confocal  
636 microscope. To perform Sholl analyses, we assessed the number of intersections of dendrite  
637 branches with four concentric circles starting from the cell body and separated by 25  $\mu\text{m}$ . The  
638 total number of intersections was normalized to the width of the larval hemi-segment, and  
639 significant changes compared with control were assessed using two-tailed Mann-Whitney tests.

640

#### 641 **Measurement of larval brain area**

642 Larval brain area was assessed in third instar larvae obtained from crosses between the RNAi  
643 lines with *Elav-GAL4*. Crosses were set up in apple plates containing yeast paste to control for  
644 size effects generated by food availability. Fifteen first instar larvae were transferred to culture  
645 vials containing a fixed volume (8-10 mL) of cornmeal-based food. Brains were dissected from  
646 third instar larva in PBS (13mM NaCl, 0.7mM Na<sub>2</sub>HPO<sub>4</sub>, and 0.3mM NaH<sub>2</sub>PO<sub>4</sub>), fixed in 4%  
647 paraformaldehyde in PBS for 20 minutes, washed three times in PBS, and mounted in Prolong  
648 Gold antifade reagent with DAPI (Thermo Fisher Scientific, P36930). Z-stacks of *Drosophila*  
649 brains were acquired every 10 $\mu\text{m}$  with a 10X air objective with 1.2X magnification using an  
650 Olympus Fluoview FV1000 laser scanning confocal microscope (Olympus America, Lake  
651 Success, NY). The area of the maximum projection of the Z-stack was measured using Fiji  
652 software (90). Differences in brain area were assessed using two-tailed Mann-Whitney tests.

653

#### 654 **RNA sequencing and differential expression analysis in *Drosophila melanogaster***

655 RNA sequencing was performed for three biological replicates of RNA isolated from 35-40  
656 *Drosophila* heads with *Elav-GAL4* mediated nervous system-specific knockdown of 16p12.1

657 homologs as well as controls with matching drivers and rearing temperatures. cDNA libraries  
658 were prepared with TruSeq Stranded mRNA LT Sample Prep Kit (Illumina, San Diego, CA).  
659 Single-end 100bp sequencing of the cDNA libraries was performed using Illumina HiSeq 2000  
660 at the Pennsylvania State University Genomics Core Facility, at an average coverage of 35.1  
661 million reads/sample. Quality control was performed using Trimmomatic (91), and raw  
662 sequencing data was aligned to the fly reference genome and transcriptome build 6.08 using  
663 TopHat2 v.2.1.1 (92). Total read counts per gene were calculated using HTSeq-Count v.0.6.1  
664 (93). Differences in gene expression were identified using a generalized linear model method in  
665 edgeR v.3.20.1 (94), with genes showing a  $\log_2$ -fold change  $>1$  or  $< -1$  and with a Benjamini-  
666 Hochberg corrected  $FDR < 0.05$  defined as differentially expressed. Human homologs of  
667 differentially-expressed genes in flies were identified using DIOPT v7.0. Biological pathways  
668 and processes affected by downregulation of homologs of 16p12.1 genes, defined as significant  
669 enrichments of Gene Ontology (GO) terms ( $p < 0.05$ , Fisher's exact test with Benjamini-  
670 Hochberg multiple testing correction), were identified using PantherDB (95).

671

### 672 **Pairwise knockdowns in the fly eye**

673 To study genetic interactions in the fly eye, we generated recombinant stock lines for each  
674 16p12.1 homolog by crossing RNAi lines with eye-specific *GMR-GAL4*, as detailed in **S1 File**.  
675 Various factors including presence of balancers, chromosomal insertion of the shRNA, lethality  
676 with *Elav-GAL4*, and severity of eye phenotypes with *GMR-GAL4* were considered to select  
677 RNAi lines for generating recombinant lines. For example, for *CG14182*, we used the GD RNAi  
678 line *CG14182<sup>GD2738</sup>*, which showed milder eye phenotypes, in order to test a wider range of  
679 potential interactions. We assessed genetic interactions between homologs of 16p12.1 genes with

680 each other as well as with homologs of “second-hits” identified in children with the 16p12.1  
681 deletion, conserved neurodevelopmental genes, and select transcriptional targets. A total of 24  
682 homologs of genes carrying “second-hits” were selected as disease-associated genes carrying  
683 rare (ExAC frequency  $\leq 1\%$ ) copy-number variants, loss-of-function (frameshift, stopgain or  
684 splicing) mutations, or *de novo* or likely-pathogenic (Phred-like CADD  $\geq 25$ ) missense mutations  
685 previously identified from exome sequencing and SNP microarrays in 15 affected children with  
686 the 16p12.1 deletion and their family members (9, 96, 97). We also selected seven conserved  
687 genes strongly associated with neurodevelopmental disorders (20, 54) and six genes with  
688 previously described functional associations with individual 16p12.1 genes, such as  
689 mitochondrial genes for *UQCRC2* (59) and *Myc* for *POLR3E* and *CDR2* (60, 61). We also tested  
690 interactions of the 16p12.1 homologs with 25 differentially-expressed genes (or “transcriptome  
691 targets”) and 14 genes selected from enriched Gene Ontology groups identified from RNA  
692 sequencing experiments (**S3 File**). Overall, we tested 212 pairwise gene interactions including 96  
693 interactions with homologs of “second-hit” genes, 55 with neurodevelopmental genes, and 61  
694 with transcriptome targets, using multiple RNAi, mutant or overexpression lines per gene when  
695 available (**S2 Table**).

696 *GMR-GAL4* recombinant lines for the homologs of 16p12.1 genes were crossed with  
697 RNAi or mutant lines for the interacting genes to achieve simultaneous knockdown of two genes  
698 in the eye. We also tested overexpression lines for specific genes that are functionally related to  
699 16p12.1 homologs, including *Myc*, *Hsp23*, and *Hsp26*. Our previous assessment showed no  
700 changes in phenotypic scores for recombinant lines crossed with *UAS-GFP* compared to crosses  
701 with controls, demonstrating that the lines have adequate *GAL4* to bind to two independent *UAS*-  
702 *RNAi* constructs (20).

703 To evaluate how simultaneous knockdown of interacting genes modulated the phenotype  
704 of 16p12.1 homologs, *Flynotyper* scores from flies with double knockdowns were compared to  
705 the scores from flies obtained from crosses between 16p12.1 recombinant lines and controls  
706 carrying the same genetic background as the interacting gene. Significant enhancements or  
707 suppressions of phenotypes of 16p12.1 homologs were identified using two-tailed Mann-  
708 Whitney tests and Benjamini-Hochberg multiple testing correction (**S3 File**).

709

### 710 **Analysis of genetic interactions using the multiplicative model**

711 The nature of genetic interactions between pairs of gene knockdowns was determined using a  
712 multiplicative model, which has been widely used for evaluating genetic interactions for  
713 quantitative phenotypes in yeast, *Drosophila*, and *E. coli* models (55-58, 98). This model tests  
714 whether the observed phenotypic effect of simultaneously knocking down two genes is different  
715 from the expected product of effects due to knockdown of individual genes. We first normalized  
716 *Flynotyper* scores for each individual line and pairwise knockdown to the *Flynotyper* scores  
717 from the background-specific controls to obtain normalized phenotypic scores as “*percentage of*  
718 *control.*” We then calculated the expected effects as the product of the averages of normalized  
719 scores for the two individual gene knockdowns, and compared the expected scores to the  
720 normalized scores from pairwise knockdowns using a two-tailed one-sample Wilcoxon signed  
721 ranked test with Benjamini-Hochberg correction. The distributions of the expected and observed  
722 values for all individual pairs of genes and pairwise knockdowns are shown in **Figure S9**.  
723 Pairwise knockdowns where the observed effects were significantly higher than expected were  
724 categorized as negative, aggravating or synergistic genetic interactions, while those with  
725 observed values significantly lower than expected were considered as positive or alleviating



726 interactions. Pairwise knockdowns where the observed effects were not significantly different  
727 from the expected effects were considered as not interacting. The magnitude of a genetic  
728 interaction was measured using “*interaction scores*”, calculated as the  $\log_2$  ratio between the  
729 observed and expected values (**S4 File**). Positive interaction scores indicated negative or  
730 aggravating genetic interactions, while negative interaction scores indicated positive or  
731 alleviating genetic interactions. An interaction was considered to be validated when the observed  
732 trend was reproduced by multiple fly lines when available. Interactions assessed with only one  
733 fly line were considered as “potential negative”, “potential positive” or “potential no interaction”  
734 (**S3 File**). To compare interactions of 16p12.1 homologs to 16p11.2 homologs, we obtained  
735 *Flynotyper* phenotypic scores from single and pairwise *GMR-GAL4*-mediated knockdown of  
736 16p11.2 homologs, previously described in Iyer *et al.* (20).

737

### 738 **Immunohistochemistry of the developing brain and eye discs in *Drosophila melanogaster***

739 Third instar larvae brain or eye discs were dissected in PBS and fixed in 4% paraformaldehyde in  
740 PBT (0.3% Triton X-100 in PBS), followed by three washes with PBT. Preparations were  
741 blocked for one hour in blocking buffer (5% FBS or 1% BSA in 0.3% PBT), followed by  
742 incubation overnight at 4°C with the primary antibody. We assessed for markers of proliferation  
743 using mouse anti-pH3 (S10) (1:100; 9706, Cell Signaling Technology, Danvers, MA, USA) and  
744 apoptosis using rabbit anti-Dcp-1 (Asp216) (1:100, 9578, Cell Signaling). Secondary antibody  
745 incubation was performed using Alexa fluor 647 goat anti-mouse (1:100, Invitrogen, Carlsbad,  
746 CA, USA) and Alexa fluor 568 goat anti-rabbit (1:100, Invitrogen) for 2 hours at 25°C, followed  
747 by three washes with PBT. Tissues were mounted in Prolong Gold antifade reagent with DAPI  
748 (Thermo Fisher Scientific, P36930) prior to imaging. Z-stacks of brain lobe or eye discs were

749 acquired every 4µm with a 40X air objective with 1.2X magnification using an Olympus  
750 Fluoview FV1000 laser scanning confocal microscope (Olympus America, Lake Success, NY).  
751 Image analysis was performed using Fiji (90). The number of cells undergoing proliferation or  
752 apoptosis were quantified throughout the brain lobe, or posterior to the morphogenetic furrow in  
753 the developing eye discs. The total number of Dcp-1 positive cells in larval brain and eye discs,  
754 as well as pH3 cells in the eye discs, were manually counted from the maximum projections. The  
755 total number of pH3 positive cells in the larval brain were quantified using the MaxEntropy  
756 automated thresholding algorithm per slice, followed by counting the number of particles larger  
757 than 1.5 µm. Differences in the number of positive pH3 or Dcp-1 cells were compared with  
758 appropriate controls using two-tailed Mann-Whitney tests.

759

#### 760 *Xenopus laevis* embryos

761 Eggs collected from female *X. laevis* frogs were fertilized *in vitro*, dejellied, and cultured  
762 following standard methods (16, 99). Embryos received injections of exogenous mRNAs or  
763 antisense oligonucleotide strategies at the two- or four-cell stage, using four total injections  
764 performed in 0.1X MMR media containing 5% Ficoll. Embryos were staged according to  
765 Nieuwkoop and Faber (100).

766

#### 767 *X. laevis* gene knockdown and rescue

768 Morpholinos (MOs) were targeted to early splice sites of *X. laevis mosmo*, *polr3e*, *uqrc2*, *cdr2*,  
769 and *setd5*, or standard control MO (S7 Table), purchased from Gene Tools (Philomath, OR). In  
770 knockdown experiments, all MOs were injected at either the 2-cell or 4-cell stage, with embryos  
771 receiving injections two or four times total. *mosmo* and control MOs were injected at 12

772 ng/embryo for partial and 20 ng/embryo for stronger knockdown; *polr3e* and control MOs were  
773 injected at 10 ng/embryo for partial and 20 ng/embryo for stronger; *uqcrc2* and control MOs  
774 were injected at 35 ng/embryo for partial and 50 ng/embryo for stronger; *cdr2* and control MOs  
775 were injected at 10 ng/embryo for partial and 20ng for stronger knockdown; and *setd5* and  
776 control MOs were injected at 10 ng/embryo for partial knockdown. All double knockdown  
777 experiments were performed with partial knockdown to avoid potential lethality.

778 Splice site MOs were validated using RT-PCR. Total RNA was extracted using Trizol  
779 reagent, followed by chloroform extraction and ethanol precipitation from 2-day old embryos  
780 injected with increasing concentrations of MO targeted to each 16p12.1 homolog, respectively.  
781 cDNA was synthesized using SuperScript II Reverse Transcriptase (Invitrogen, Carlsbad, CA,  
782 USA). PCR was performed in a Mastercycler using HotStarTaq DNA Polymerase (Qiagen,  
783 Germantown, MD, USA) following manufacturer instructions. PCR was performed using  
784 primers with sequences detailed in **S6 Table**. RT-PCR was performed in triplicate, and band  
785 intensity was measured using the densitometry function in ImageJ (101) and normalized to the  
786 uninjected control mean relative to the housekeeping control *odc1*. Phenotypes were rescued  
787 with exogenous mRNAs co-injected with their corresponding MO strategies. *X. laevis* ORF for  
788 *mosmo* was purchased from the European *Xenopus* Resource Center (EXRC, Portsmouth, UK)  
789 and gateway-cloned into pCSF107mT-GATEWAY-3'GFP destination vector. Constructs used  
790 were *mosmo*-GFP, and GFP in pCS2+. In rescue experiments, MOs of the same amount used as  
791 for the knockdown of each homolog were co-injected along with mRNA (1000pg/embryo for  
792 *mosmo*-GFP) in the same injection solution.

793

794 **Quantifying craniofacial shape and size of *X. laevis* embryos**

795 The protocol for quantifying craniofacial shape and size was adapted from Kennedy and  
796 Dickinson (102). Embryos at stage 42 were fixed overnight in 4% paraformaldehyde in PBS. A  
797 razor blade was used to make a cut bisecting the gut to isolate the head. Isolated heads were  
798 mounted in small holes in a clay-lined dish containing PBS. Frontal and lateral view images were  
799 taken using a Zeiss AxioCam MRc attached to a Zeiss SteREO Discovery.V8 light microscope  
800 (Zeiss, Thornwood, NY, USA). ImageJ software (101) was used to perform craniofacial  
801 measurements, including: 1) facial width, which is the distance between the eyes; 2) face height,  
802 which is the distance between the top of the eyes and the top of the cement gland at the midline;  
803 3) dorsal mouth angle, which is the angle created by drawing lines from the center of one eye, to  
804 the dorsal midline of the mouth, to the center of the opposite eye; and 4) midface area, which is  
805 the area measured from the top of the eyes to the cement gland encircling the edges of both eyes.  
806 For all facial measurements, two-tailed student's t-tests were performed between knockdown  
807 embryos and control MO-injected embryos with the same amount of morpholino.

808

### 809 **Neural tube explants, imaging, and analysis**

810 Embryos were injected with either control MO or 16p12.1 homolog-specific MO at the 2-4 cell  
811 stage, and culturing of *Xenopus* embryonic neural tube explants from stage 20-22 embryos were  
812 performed as previously described (99). For axon outgrowth analysis, phase contrast images of  
813 axons were collected on a Zeiss Axio Observer inverted motorized microscope with a Zeiss  
814 20X/0.5 Plan Apo phase objective (Zeiss, Thornwood, NY, USA). Raw images were analyzed by  
815 manually tracing the length of individual axons using the NeuronJ plug-in in ImageJ (103). All  
816 experiments were performed on multiple independent occasions to ensure reproducibility. Axon  
817 outgrowth data were normalized to controls from the same experiment to account for day-to-day

818 fluctuations. Statistical differences were identified between knockdown embryos and control  
819 MO-injected embryos with same amounts of morpholino using two-tailed student's t-tests.

820

### 821 **Immunostaining for brain morphology, imaging, and analysis**

822 For brain morphology analysis, half embryo KDs were performed at the two-cell stage. *X. laevis*  
823 embryos were unilaterally injected two times with either control MO or 16p12.1 homolog-  
824 specific MO and a GFP mRNA construct (300pg/embryo). The other blastomere was left  
825 uninjected. Embryos were raised in 0.1X MMR through neurulation, and then sorted based on  
826 left/right fluorescence. Stage 47 embryos were fixed in 4% paraformaldehyde diluted in PBS for  
827 one hour, rinsed in PBS, and gutted to reduce autofluorescence. Embryos were processed for  
828 immunoreactivity by incubating in 3% bovine serum albumin and 1% Triton-X 100 in PBS for  
829 two hours, and then incubated in anti-acetylated tubulin (1:700, T7451SigmaAldrich, St. Louis  
830 MO, USA) and goat anti-mouse Alexa Fluor 488 conjugate secondary antibody (1:1000,  
831 Invitrogen, Carlsbad, CA, USA). Embryos were rinsed in 1% Tween-20 in PBS and imaged in  
832 PBS. Removal of the skin dorsal to the brain was performed if the brain was not clearly visible  
833 due to pigment.

834 Images were taken at 3.2X magnification using a Zeiss AxioCam MRc attached to a  
835 Zeiss SteREO Discovery.V8 light microscope (Zeiss, Thornwood, NY, USA). Images were  
836 processed in ImageJ (101). The areas of the forebrain and midbrain were determined from raw  
837 images using the polygon area function in ImageJ. Brain sizes were quantified by taking the ratio  
838 of forebrain and midbrain areas between the injected side versus the uninjected side for each  
839 sample. All experiments were performed on at least three independent occasions to ensure  
840 reproducibility, and data shown represent findings from multiple replicates. Statistical

841 differences were identified between knockdown embryos and control MO injected embryos with  
842 the same amount of morpholino using two-tailed student's t-tests.

843

#### 844 **Western blot for cell proliferation**

845 Embryos at stage 20 to 22 were lysed in buffer (50mM Tris pH 7.5, 1% NP40, 150mM NaCl,  
846 1mM PMSF, 0.5 mM EDTA), supplemented with cOmplete™ Mini EDTA-free Protease  
847 Inhibitor Cocktail (Sigma-Aldrich) and PhosSTOP™ Phosphatase Inhibitor Cocktail (Sigma-  
848 Aldrich). Blotting was carried out using rabbit polyclonal antibody to Phospho-Histone H3  
849 (Ser10) (1:500, PA5-17869, Invitrogen), with mouse anti-beta actin (1:2500, ab8224, Abcam,  
850 Cambridge, MA, USA) as a loading control. Bands were detected by chemiluminescence using  
851 Amersham ECL Western blot reagent (GE Healthcare Bio-Sciences, Pittsburgh, PA). Band  
852 intensities were quantified by densitometry in ImageJ and normalized to the control mean  
853 relative to  $\beta$ -actin.

854

#### 855 **Connectivity of 16p12.1 and 16p11.2 deletion genes in a human brain-specific interaction** 856 **network**

857 We examined the connectivity of human 16p12.1 and 16p11.2 deletion genes in the context of a  
858 human brain-specific gene interaction network that was previously built using a Bayesian  
859 classifier trained on gene co-expression datasets (71, 72). As the classifier assigned weighted  
860 probabilities for interactions between all possible pairs of genes in the genome, we first built a  
861 network that only contained the top 0.5% of all pairwise interactions (predicted weights >2.0).  
862 Within this network, we identified the shortest paths between each 16p11.2 or 16p12.1 gene and  
863 all other protein-coding genes in the genome, using the inverse of the probabilities as weights for

864 each interaction. For each shortest path, we calculated the overall length as a measure of  
865 connectivity between the two genes, and also identified the connector genes located within the  
866 shortest path. All network analyses were performed using the NetworkX v.2.4 Python package  
867 (104). We compared the average connectivity of 16p12.1 genes to 16p11.2 genes, as well as the  
868 predicted pathogenicity of connector genes for 16p11.2 and 16p12.1 interactions, using two-  
869 tailed Mann-Whitney tests.

870

### 871 **Statistical analyses**

872 All statistical analyses of functional data were performed using R v.3.4.2 (R Foundation for  
873 Statistical Computing, Vienna, Austria). Details for each statistical test, including sample size, p-  
874 values with and without multiple testing correction, confidence intervals, test statistics, and  
875 ANOVA degrees of freedom, are provided in **S6 File**.

876

877 **Data access**

878 Gene expression data for the *Drosophila* RNAi knockdown of homologs of 16p12.1 genes and  
879 controls have been submitted to the NCBI Gene Expression Omnibus (GEO;  
880 <https://www.ncbi.nlm.nih.gov/geo/>) under accession number GSE151330, and the raw RNA  
881 Sequencing files are deposited in the SRA (Sequence Read Archive) with BioProject database  
882 (<https://www.ncbi.nlm.nih.gov/bioproject/>) accession number PRJNA635495. Source code for  
883 the RNA-Sequencing and network analysis is available on the Girirajan lab GitHub page at  
884 [https://github.com/girirajanlab/16p12\\_fly\\_project](https://github.com/girirajanlab/16p12_fly_project).

885

886 **Acknowledgments**

887 This work was supported by NIH R01GM121907 and resources from the Huck Institutes of the  
888 Life Sciences to S.G, Fulbright Commission Uruguay-ANII to L.P, NIH T32-GM102057 to  
889 M.J., and NIH R01GM085115 to M.M.R.

890

891 **Disclosure declaration**

892 Authors disclose no conflict of interest.

893



## 894 **References**

- 895 1. Girirajan S, Campbell CD, Eichler EE. Human copy number variation and complex genetic  
896 disease. *Annu Rev Genet.* 2011;45:203-26.
- 897 2. Wilfert AB, Sulovari A, Turner TN, Coe BP, Eichler EE. Recurrent de novo mutations in  
898 neurodevelopmental disorders: properties and clinical implications. *Genome Med.* 2017;9(1):101.
- 899 3. Weiss LA, Shen Y, Korn JM, Arking DE, Miller DT, Fossdal R, et al. Association between  
900 microdeletion and microduplication at 16p11.2 and autism. *N Engl J Med.* 2008;358(7):667-75.
- 901 4. Zufferey F, Sherr EH, Beckmann ND, Hanson E, Maillard AM, Hippolyte L, et al. A 600 kb  
902 deletion syndrome at 16p11. 2 leads to energy imbalance and neuropsychiatric disorders. *Journal of*  
903 *medical genetics.* 2012;49(10):660-8.
- 904 5. Mulle JG. The 3q29 deletion confers >40-fold increase in risk for schizophrenia. *Mol Psychiatry.*  
905 2015;20(9):1028-9.
- 906 6. Helbig I, Mefford HC, Sharp AJ, Guipponi M, Fichera M, Franke A, et al. 15q13.3  
907 microdeletions increase risk of idiopathic generalized epilepsy. *Nat Genet.* 2009;41(2):160-2.
- 908 7. Girirajan S, Eichler EE. Phenotypic variability and genetic susceptibility to genomic disorders.  
909 *Human molecular genetics.* 2010;19(R2):R176-R87.
- 910 8. Girirajan S, Rosenfeld JA, Cooper GM, Antonacci F, Siswara P, Itsara A, et al. A recurrent  
911 16p12. 1 microdeletion supports a two-hit model for severe developmental delay. *Nature genetics.*  
912 2010;42(3):203-9.
- 913 9. Pizzo L, Jensen M, Polyak A, Rosenfeld JA, Mannik K, Krishnan A, et al. Rare variants in the  
914 genetic background modulate cognitive and developmental phenotypes in individuals carrying disease-  
915 associated variants. *Genet Med.* 2018.
- 916 10. Stefansson H, Meyer-Lindenberg A, Steinberg S, Magnusdottir B, Morgen K, Arnarsdottir S, et  
917 al. CNVs conferring risk of autism or schizophrenia affect cognition in controls. *Nature.*  
918 2014;505(7483):361-6.
- 919 11. Girirajan S, Rosenfeld JA, Coe BP, Parikh S, Friedman N, Goldstein A, et al. Phenotypic  
920 heterogeneity of genomic disorders and rare copy-number variants. *New England Journal of Medicine.*  
921 2012;367(14):1321-31.
- 922 12. Gatto CL, Pereira D, Broadie K. GABAergic circuit dysfunction in the Drosophila Fragile X  
923 syndrome model. *Neurobiol Dis.* 2014;65:142-59.
- 924 13. Jumbo-Lucioni PP, Parkinson WM, Kopke DL, Broadie K. Coordinated movement,  
925 neuromuscular synaptogenesis and trans-synaptic signaling defects in Drosophila galactosemia models.  
926 *Hum Mol Genet.* 2016;25(17):3699-714.
- 927 14. Sears JC, Broadie K. Fragile X Mental Retardation Protein Regulates Activity-Dependent  
928 Membrane Trafficking and Trans-Synaptic Signaling Mediating Synaptic Remodeling. *Front Mol*  
929 *Neurosci.* 2017;10:440.
- 930 15. Grossman TR, Gamliel A, Wessells RJ, Taghli-Lamalle O, Jepsen K, Ocorr K, et al. Over-  
931 expression of DSCAM and COL6A2 cooperatively generates congenital heart defects. *PLoS Genet.*  
932 2011;7(11):e1002344.
- 933 16. Chen SX, Tari PK, She K, Haas K. Neurexin-neurologin cell adhesion complexes contribute to  
934 synaptotropic dendritogenesis via growth stabilization mechanisms in vivo. *Neuron.* 2010;67(6):967-83.
- 935 17. Lewis BB, Wester MR, Miller LE, Nagarkar MD, Johnson MB, Saha MS. Cloning and  
936 characterization of voltage-gated calcium channel  $\alpha 1$  subunits in *Xenopus laevis* during development.  
937 *Dev Dyn.* 2009;238(11):2891-902.
- 938 18. Ishimaru H, Kamboj R, Ambrosini A, Henley JM, Soloviev MM, Sudan H, et al. A unitary non-  
939 NMDA receptor short subunit from *Xenopus*: DNA cloning and expression. *Receptors Channels.*  
940 1996;4(1):31-49.
- 941 19. Ueno S, Kono R, Iwao Y. PTEN is required for the normal progression of gastrulation by  
942 repressing cell proliferation after MBT in *Xenopus* embryos. *Dev Biol.* 2006;297(1):274-83.

- 943 20. Iyer J, Singh MD, Jensen M, Patel P, Pizzo L, Huber E, et al. Pervasive genetic interactions  
944 modulate neurodevelopmental defects of the autism-associated 16p11.2 deletion in *Drosophila*  
945 *melanogaster*. *Nat Commun*. 2018;9(1):2548.
- 946 21. Singh MD, Jensen M, Lasser M, Huber E, Yusuff T, Pizzo L, et al. NCBP2 modulates  
947 neurodevelopmental defects of the 3q29 deletion in *Drosophila* and *Xenopus laevis* models. *PLoS Genet*.  
948 2020;16(2):e1008590.
- 949 22. McCammon JM, Blaker-Lee A, Chen X, Sive H. The 16p11.2 homologs *fam57ba* and *doc2a*  
950 generate certain brain and body phenotypes. *Hum Mol Genet*. 2017;26(19):3699-712.
- 951 23. Qiu Y, Arbogast T, Lorenzo SM, Li H, Tang SC, Richardson E, et al. Oligogenic Effects of  
952 16p11.2 Copy-Number Variation on Craniofacial Development. *Cell Rep*. 2019;28(13):3320-8 e4.
- 953 24. Hu Y, Flockhart I, Vinayagam A, Bergwitz C, Berger B, Perrimon N, et al. An integrative  
954 approach to ortholog prediction for disease-focused and other functional studies. *BMC Bioinformatics*.  
955 2011;12:357.
- 956 25. Brand AH, Perrimon N. Targeted gene expression as a means of altering cell fates and generating  
957 dominant phenotypes. *Development*. 1993;118(2):401-15.
- 958 26. Strigini M, Cohen SM. A Hedgehog activity gradient contributes to AP axial patterning of the  
959 *Drosophila* wing. *Development*. 1997;124(22):4697-705.
- 960 27. Yan SJ, Gu Y, Li WX, Fleming RJ. Multiple signaling pathways and a selector protein  
961 sequentially regulate *Drosophila* wing development. *Development*. 2004;131(2):285-98.
- 962 28. Yusuff T, Jensen M, Yennawar S, Pizzo L, Karthikeyan S, Gould DJ, et al. *Drosophila* models of  
963 pathogenic copy-number variant genes show global and non-neuronal defects during development. *PLoS*  
964 *Genet*. 2020;16(6):e1008792.
- 965 29. Callan MA, Cabernard C, Heck J, Luois S, Doe CQ, Zarnescu DC. Fragile X protein controls  
966 neural stem cell proliferation in the *Drosophila* brain. *Hum Mol Genet*. 2010;19(15):3068-79.
- 967 30. Kwon CH, Luikart BW, Powell CM, Zhou J, Matheny SA, Zhang W, et al. Pten regulates  
968 neuronal arborization and social interaction in mice. *Neuron*. 2006;50(3):377-88.
- 969 31. Lee A, Li W, Xu K, Bogert BA, Su K, Gao FB. Control of dendritic development by the  
970 *Drosophila* fragile X-related gene involves the small GTPase Rac1. *Development*. 2003;130(22):5543-52.
- 971 32. Parker L, Padilla M, Du Y, Dong K, Tanouye MA. *Drosophila* as a model for epilepsy: *bss* is a  
972 gain-of-function mutation in the para sodium channel gene that leads to seizures. *Genetics*.  
973 2011;187(2):523-34.
- 974 33. Rujano MA, Sanchez-Pulido L, Pannetier C, le Dez G, Basto R. The microcephaly protein *Asp*  
975 regulates neuroepithelium morphogenesis by controlling the spatial distribution of myosin II. *Nat Cell*  
976 *Biol*. 2013;15(11):1294-306.
- 977 34. Stuss DP, Boyd JD, Levin DB, Delaney KR. *MeCP2* mutation results in compartment-specific  
978 reductions in dendritic branching and spine density in layer 5 motor cortical neurons of YFP-H mice.  
979 *PLoS One*. 2012;7(3):e31896.
- 980 35. Wang HD, Kazemi-Esfarjani P, Benzer S. Multiple-stress analysis for isolation of *Drosophila*  
981 longevity genes. *Proc Natl Acad Sci U S A*. 2004;101(34):12610-5.
- 982 36. Orr WC, Sohal RS. Extension of life-span by overexpression of superoxide dismutase and  
983 catalase in *Drosophila melanogaster*. *Science*. 1994;263(5150):1128-30.
- 984 37. Copeland JM, Cho J, Lo T, Jr., Hur JH, Bahadorani S, Arabyan T, et al. Extension of *Drosophila*  
985 life span by RNAi of the mitochondrial respiratory chain. *Curr Biol*. 2009;19(19):1591-8.
- 986 38. Mahmoudi S, Xu L, Brunet A. Turning back time with emerging rejuvenation strategies. *Nat Cell*  
987 *Biol*. 2019;21(1):32-43.
- 988 39. Matthews BJ, Kim ME, Flanagan JJ, Hattori D, Clemens JC, Zipursky SL, et al. Dendrite self-  
989 avoidance is controlled by *Dscam*. *Cell*. 2007;129(3):593-604.
- 990 40. Soba P, Zhu S, Emoto K, Younger S, Yang SJ, Yu HH, et al. *Drosophila* sensory neurons require  
991 *Dscam* for dendritic self-avoidance and proper dendritic field organization. *Neuron*. 2007;54(3):403-16.
- 992 41. King KL, Cidlowski JA. Cell cycle and apoptosis: common pathways to life and death. *J Cell*  
993 *Biochem*. 1995;58(2):175-80.

- 994 42. King KL, Cidlowski JA. Cell cycle regulation and apoptosis. *Annu Rev Physiol.* 1998;60:601-17.  
995 43. Hunt P, Gulisano M, Cook M, Sham MH, Faiella A, Wilkinson D, et al. A distinct Hox code for  
996 the branchial region of the vertebrate head. *Nature.* 1991;353(6347):861-4.  
997 44. Hunt P, Whiting J, Muchamore I, Marshall H, Krumlauf R. Homeobox genes and models for  
998 patterning the hindbrain and branchial arches. *Dev Suppl.* 1991;1:187-96.  
999 45. Lasser M, Pratt B, Monahan C, Kim SW, Lowery LA. The Many Faces of *Xenopus*: *Xenopus*  
1000 *laevis* as a Model System to Study Wolf-Hirschhorn Syndrome. *Front Physiol.* 2019;10:817.  
1001 46. Le Lievre CS, Le Douarin NM. Mesenchymal derivatives of the neural crest: analysis of  
1002 chimaeric quail and chick embryos. *J Embryol Exp Morphol.* 1975;34(1):125-54.  
1003 47. Lumsden A, Sprawson N, Graham A. Segmental origin and migration of neural crest cells in the  
1004 hindbrain region of the chick embryo. *Development.* 1991;113(4):1281-91.  
1005 48. Mills A, Bearce E, Cella R, Kim SW, Selig M, Lee S, et al. Wolf-Hirschhorn Syndrome-  
1006 Associated Genes Are Enriched in Motile Neural Crest Cells and Affect Craniofacial Development in  
1007 *Xenopus laevis*. *Front Physiol.* 2019;10:431.  
1008 49. Goldberg JL. How does an axon grow? *Genes Dev.* 2003;17(8):941-58.  
1009 50. Jensen M, Girirajan S. An interaction-based model for neuropsychiatric features of copy-number  
1010 variants. *PLoS Genet.* 2019;15(1):e1007879.  
1011 51. Thaker HM, Kankel DR. Mosaic analysis gives an estimate of the extent of genomic involvement  
1012 in the development of the visual system in *Drosophila melanogaster*. *Genetics.* 1992;131(4):883-94.  
1013 52. Branco J, Al-Ramahi I, Ukani L, Perez AM, Fernandez-Funez P, Rincon-Limas D, et al.  
1014 Comparative analysis of genetic modifiers in *Drosophila* points to common and distinct mechanisms of  
1015 pathogenesis among polyglutamine diseases. *Hum Mol Genet.* 2008;17(3):376-90.  
1016 53. Cziko AM, McCann CT, Howlett IC, Barbee SA, Duncan RP, Luedemann R, et al. Genetic  
1017 modifiers of dFMR1 encode RNA granule components in *Drosophila*. *Genetics.* 2009;182(4):1051-60.  
1018 54. Iyer J, Wang Q, Le T, Pizzo L, Gronke S, Ambegaokar SS, et al. Quantitative Assessment of Eye  
1019 Phenotypes for Functional Genetic Studies Using *Drosophila melanogaster*. *G3 (Bethesda).*  
1020 2016;6(5):1427-37.  
1021 55. Baryshnikova A, Costanzo M, Kim Y, Ding H, Koh J, Toufighi K, et al. Quantitative analysis of  
1022 fitness and genetic interactions in yeast on a genome scale. *Nat Methods.* 2010;7(12):1017-24.  
1023 56. Dixon SJ, Costanzo M, Baryshnikova A, Andrews B, Boone C. Systematic mapping of genetic  
1024 interaction networks. *Annu Rev Genet.* 2009;43:601-25.  
1025 57. Horn T, Sandmann T, Fischer B, Axelsson E, Huber W, Boutros M. Mapping of signaling  
1026 networks through synthetic genetic interaction analysis by RNAi. *Nat Methods.* 2011;8(4):341-6.  
1027 58. Jonikas MC, Collins SR, Denic V, Oh E, Quan EM, Schmid V, et al. Comprehensive  
1028 characterization of genes required for protein folding in the endoplasmic reticulum. *Science.*  
1029 2009;323(5922):1693-7.  
1030 59. Duncan AM, Ozawa T, Suzuki H, Rozen R. Assignment of the gene for the core protein II  
1031 (UQCRC2) subunit of the mitochondrial cytochrome bc1 complex to human chromosome 16p12.  
1032 *Genomics.* 1993;18(2):455-6.  
1033 60. Gomez-Roman N, Grandori C, Eisenman RN, White RJ. Direct activation of RNA polymerase III  
1034 transcription by c-Myc. *Nature.* 2003;421(6920):290-4.  
1035 61. O'Donovan KJ, Diedler J, Couture GC, Fak JJ, Darnell RB. The onconeural antigen *cdr2* is a  
1036 novel APC/C target that acts in mitosis to regulate c-myc target genes in mammalian tumor cells. *PLoS*  
1037 *One.* 2010;5(4):e10045.  
1038 62. Hartman JLt, Garvik B, Hartwell L. Principles for the buffering of genetic variation. *Science.*  
1039 2001;291(5506):1001-4.  
1040 63. Queitsch C, Carlson KD, Girirajan S. Lessons from model organisms: phenotypic robustness and  
1041 missing heritability in complex disease. *PLoS Genet.* 2012;8(11):e1003041.  
1042 64. Grozeva D, Carss K, Spasic-Boskovic O, Parker MJ, Archer H, Firth HV, et al. De novo loss-of-  
1043 function mutations in SETD5, encoding a methyltransferase in a 3p25 microdeletion syndrome critical  
1044 region, cause intellectual disability. *Am J Hum Genet.* 2014;94(4):618-24.

- 1045 65. Hu P, Wu S, Sun Y, Yuan CC, Kobayashi R, Myers MP, et al. Characterization of human RNA  
1046 polymerase III identifies orthologues for *Saccharomyces cerevisiae* RNA polymerase III subunits. *Mol*  
1047 *Cell Biol.* 2002;22(22):8044-55.
- 1048 66. Pusapati GV, Kong JH, Patel BB, Krishnan A, Sagner A, Kinnebrew M, et al. CRISPR Screens  
1049 Uncover Genes that Regulate Target Cell Sensitivity to the Morphogen Sonic Hedgehog. *Dev Cell.*  
1050 2018;44(2):271.
- 1051 67. McCamphill PK, Farah CA, Anadolu MN, Hoque S, Sossin WS. Bidirectional regulation of eEF2  
1052 phosphorylation controls synaptic plasticity by decoding neuronal activity patterns. *J Neurosci.*  
1053 2015;35(10):4403-17.
- 1054 68. Gildish I, Manor D, David O, Sharma V, Williams D, Agarwala U, et al. Impaired associative  
1055 taste learning and abnormal brain activation in kinase-defective eEF2K mice. *Learn Mem.*  
1056 2012;19(3):116-25.
- 1057 69. Zhang P, Riazzy M, Gold M, Tsai SH, McNagny K, Proud C, et al. Impairing eukaryotic  
1058 elongation factor 2 kinase activity decreases atherosclerotic plaque formation. *Can J Cardiol.*  
1059 2014;30(12):1684-8.
- 1060 70. Monteggia LM, Gideons E, Kavalali ET. The role of eukaryotic elongation factor 2 kinase in  
1061 rapid antidepressant action of ketamine. *Biol Psychiatry.* 2013;73(12):1199-203.
- 1062 71. Greene CS, Krishnan A, Wong AK, Ricciotti E, Zelaya RA, Himmelstein DS, et al.  
1063 Understanding multicellular function and disease with human tissue-specific networks. *Nat Genet.*  
1064 2015;47(6):569-76.
- 1065 72. Krishnan A, Zhang R, Yao V, Theesfeld CL, Wong AK, Tadych A, et al. Genome-wide  
1066 prediction and functional characterization of the genetic basis of autism spectrum disorder. *Nat Neurosci.*  
1067 2016;19(11):1454-62.
- 1068 73. Osipovich AB, Gangula R, Vianna PG, Magnuson MA. Setd5 is essential for mammalian  
1069 development and the co-transcriptional regulation of histone acetylation. *Development.*  
1070 2016;143(24):4595-607.
- 1071 74. Andrews T, Honti F, Pfundt R, de Leeuw N, Hehir-Kwa J, Vulto-van Silfhout A, et al. The  
1072 clustering of functionally related genes contributes to CNV-mediated disease. *Genome Res.*  
1073 2015;25(6):802-13.
- 1074 75. Iossifov I, Levy D, Allen J, Ye K, Ronemus M, Lee YH, et al. Low load for disruptive mutations  
1075 in autism genes and their biased transmission. *Proc Natl Acad Sci U S A.* 2015;112(41):E5600-7.
- 1076 76. Kury S, van Woerden GM, Besnard T, Proietti Onori M, Latypova X, Towne MC, et al. De Novo  
1077 Mutations in Protein Kinase Genes CAMK2A and CAMK2B Cause Intellectual Disability. *Am J Hum*  
1078 *Genet.* 2017;101(5):768-88.
- 1079 77. Krumm N, Turner TN, Baker C, Vives L, Mohajeri K, Witherspoon K, et al. Excess of rare,  
1080 inherited truncating mutations in autism. *Nature genetics.* 2015;47(6):582-8.
- 1081 78. Petrovski S, Wang Q, Heinzen EL, Allen AS, Goldstein DB. Genic intolerance to functional  
1082 variation and the interpretation of personal genomes. *PLoS Genet.* 2013;9(8):e1003709.
- 1083 79. Yates AD, Achuthan P, Akanni W, Allen J, Allen J, Alvarez-Jarreta J, et al. Ensembl 2020.  
1084 *Nucleic Acids Res.* 2020;48(D1):D682-D8.
- 1085 80. Altschul SF, Madden TL, Schaffer AA, Zhang J, Zhang Z, Miller W, et al. Gapped BLAST and  
1086 PSI-BLAST: a new generation of protein database search programs. *Nucleic Acids Res.*  
1087 1997;25(17):3389-402.
- 1088 81. Chintapalli VR, Wang J, Dow JA. Using FlyAtlas to identify better *Drosophila melanogaster*  
1089 models of human disease. *Nat Genet.* 2007;39(6):715-20.
- 1090 82. Bowes JB, Snyder KA, Segerdell E, Jarabek CJ, Azam K, Zorn AM, et al. Xenbase: gene  
1091 expression and improved integration. *Nucleic Acids Res.* 2010;38(Database issue):D607-12.
- 1092 83. Xu D, Wang Y, Willecke R, Chen Z, Ding T, Bergmann A. The effector caspases drICE and dcp-  
1093 1 have partially overlapping functions in the apoptotic pathway in *Drosophila*. *Cell Death Differ.*  
1094 2006;13(10):1697-706.

- 1095 84. Schmid A, Hallermann S, Kittel RJ, Khorramshahi O, Frolich AM, Quentin C, et al. Activity-  
1096 dependent site-specific changes of glutamate receptor composition in vivo. *Nat Neurosci*.  
1097 2008;11(6):659-66.
- 1098 85. Xiao C, Mileva-Seitz V, Seroude L, Robertson RM. Targeting HSP70 to motoneurons protects  
1099 locomotor activity from hyperthermia in *Drosophila*. *Dev Neurobiol*. 2007;67(4):438-55.
- 1100 86. Ye J, Coulouris G, Zaretskaya I, Cutcutache I, Rozen S, Madden TL. Primer-BLAST: a tool to  
1101 design target-specific primers for polymerase chain reaction. *BMC Bioinformatics*. 2012;13:134.
- 1102 87. Livak KJ, Schmittgen TD. Analysis of relative gene expression data using real-time quantitative  
1103 PCR and the 2<sup>-Delta Delta C(T)</sup> Method. *Methods*. 2001;25(4):402-8.
- 1104 88. Sun Y, Yolitz J, Wang C, Spangler E, Zhan M, Zou S. Aging studies in *Drosophila melanogaster*.  
1105 *Methods Mol Biol*. 2013;1048:77-93.
- 1106 89. Ganetzky B, Wu CF. Indirect Suppression Involving Behavioral Mutants with Altered Nerve  
1107 Excitability in *DROSOPHILA MELANOGASTER*. *Genetics*. 1982;100(4):597-614.
- 1108 90. Schindelin J, Arganda-Carreras I, Frise E, Kaynig V, Longair M, Pietzsch T, et al. Fiji: an open-  
1109 source platform for biological-image analysis. *Nat Methods*. 2012;9(7):676-82.
- 1110 91. Bolger AM, Lohse M, Usadel B. Trimmomatic: a flexible trimmer for Illumina sequence data.  
1111 *Bioinformatics*. 2014;30(15):2114-20.
- 1112 92. Kim D, Pertea G, Trapnell C, Pimentel H, Kelley R, Salzberg SL. TopHat2: accurate alignment  
1113 of transcriptomes in the presence of insertions, deletions and gene fusions. *Genome Biol*. 2013;14(4):R36.
- 1114 93. Anders S, Pyl PT, Huber W. HTSeq--a Python framework to work with high-throughput  
1115 sequencing data. *Bioinformatics*. 2015;31(2):166-9.
- 1116 94. Robinson MD, McCarthy DJ, Smyth GK. edgeR: a Bioconductor package for differential  
1117 expression analysis of digital gene expression data. *Bioinformatics*. 2010;26(1):139-40.
- 1118 95. Thomas PD, Campbell MJ, Kejariwal A, Mi H, Karlak B, Daverman R, et al. PANTHER: a  
1119 library of protein families and subfamilies indexed by function. *Genome Res*. 2003;13(9):2129-41.
- 1120 96. Kircher M, Witten DM, Jain P, O'Roak BJ, Cooper GM, Shendure J. A general framework for  
1121 estimating the relative pathogenicity of human genetic variants. *Nat Genet*. 2014;46(3):310-5.
- 1122 97. Lek M, Karczewski KJ, Minikel EV, Samocha KE, Banks E, Fennell T, et al. Analysis of protein-  
1123 coding genetic variation in 60,706 humans. *Nature*. 2016;536(7616):285-91.
- 1124 98. Elena SF, Lenski RE. Test of synergistic interactions among deleterious mutations in bacteria.  
1125 *Nature*. 1997;390(6658):395-8.
- 1126 99. Lowery LA, Faris AE, Stout A, Van Vactor D. Neural Explant Cultures from *Xenopus laevis*. *J*  
1127 *Vis Exp*. 2012(68):e4232.
- 1128 100. Nieuwkoop PD FJ. Normal table of *Xenopus laevis* (Daudin) : a systematical and chronological  
1129 survey of the development from the fertilized egg till the end of metamorphosis: Garland Pub., 1994;  
1130 1994.
- 1131 101. Schneider CA, Rasband WS, Eliceiri KW. NIH Image to ImageJ: 25 years of image analysis. *Nat*  
1132 *Methods*. 2012;9(7):671-5.
- 1133 102. Kennedy AE, Dickinson AJ. Quantitative analysis of orofacial development and median clefts in  
1134 *Xenopus laevis*. *Anat Rec (Hoboken)*. 2014;297(5):834-55.
- 1135 103. Popko J, Fernandes A, Brites D, Lanier LM. Automated analysis of NeuronJ tracing data.  
1136 *Cytometry A*. 2009;75(4):371-6.
- 1137 104. Hagberg AA SD, Swart PJ, editor *Exploring network structure, dynamics, and function using*  
1138 *NetworkX*.  
1139 7th Python in Science Conference SciPy 2008; 2008.
- 1140 105. D'Angelo D, Lebon S, Chen Q, Martin-Brevet S, Snyder LG, Hippolyte L, et al. Defining the  
1141 Effect of the 16p11.2 Duplication on Cognition, Behavior, and Medical Comorbidities. *JAMA Psychiatry*.  
1142 2016;73(1):20-30.
- 1143 106. Niarchou M, Chawner S, Doherty JL, Maillard AM, Jacquemont S, Chung WK, et al. Psychiatric  
1144 disorders in children with 16p11.2 deletion and duplication. *Transl Psychiatry*. 2019;9(1):8.  
1145

## 1146 **Figure Legends**

### 1147 **Fig. 1. Strategy to evaluate the individual contributions of homologs of 16p12.1 genes and** 1148 **their interactions with “second-hit” genes towards neurodevelopmental phenotypes. (A)**

1149 Ideogram of human chromosome 16 indicating the deleted region on UCSC genome build  
1150 GRCh37, hg19 (chr16:21,948,445-22,430,408) (also known as 16p12.2 deletion). Seven protein  
1151 coding genes are located within the 16p12.1 deletion region, including *UQCRC2*, *PDZD9*,  
1152 *MOSMO*, *VWA3A*, *EEF2K*, *POLR3E*, and *CDR2*. Four out of the seven genes are conserved in  
1153 both *Drosophila melanogaster* and *Xenopus laevis*. **(B)** We performed global and functional  
1154 domain-specific phenotypic assessment using RNAi lines and tissue-specific knockdown in  
1155 *Drosophila*, and morpholino-mediated whole embryo knockdown in *X. laevis*, to identify  
1156 individual contributions of 16p12.1 homologs towards different developmental and neuronal  
1157 features. We next evaluated the effect of pairwise knockdown of 16p12.1 homologs towards eye  
1158 phenotypes in *Drosophila*, and brain size and cellular proliferation defects in *X. laevis*. We  
1159 characterized 212 interactions between the 16p12.1 homologs and homologs of patient-specific  
1160 “second-hit” genes identified in children with the deletion, genes within conserved  
1161 neurodevelopmental pathways, and differentially-expressed genes identified from RNA-seq  
1162 analysis. We found that homologs of “second-hit” genes participate in complex genetic  
1163 interactions with 16p12.1 homologs to modulate neurodevelopmental and cellular phenotypes.

1164

### 1165 **Fig. 2. Multiple homologs of 16p12.1 genes contribute to neurodevelopmental defects in** 1166 ***Drosophila melanogaster* and *X. laevis*.**

1167 **(A)** Schematic showing multiple phenotypes affected by tissue-specific knockdown of individual  
1168 16p12.1 homologs in *Drosophila melanogaster*. Ubiquitous knockdown was achieved with *da-*

1169 *GAL4*, eye-specific knockdown with *GMR-GAL4*, wing-specific knockdown with *bx<sup>MS1096</sup>* -  
1170 *GAL4*, and nervous system-specific with *ppk-GAL4* or *Elav-GAL4*. See **S2A-C Figure** for details  
1171 on phenotypes observed for individual fly lines. **(B)** Nervous-system mediated knockdown using  
1172 *Elav-GAL4* with overexpression of *Dicer2* at 25°C led to reduced lifespan with knockdown of  
1173 *CG14182<sup>GD2738\_2</sup>* (n=100, one-way repeat measures ANOVA with post-hoc pairwise t-test, days  
1174 6-61, p<0.05) and increased lifespan with knockdown of *UQCR-C2<sup>GD11238</sup>* (n=120, days 51-81,  
1175 p<0.05). *Elav-GAL4* mediated knockdown of *Sin<sup>GD7027</sup>* at RT without overexpression of *Dicer2*  
1176 led to reduced lifespan of adult flies (n=160, day 1-6, p<0.05). Data represented show mean ±  
1177 standard deviation of 4-8 independent groups of 20 flies for each line tested. **(C)** Nervous-system  
1178 mediated knockdown led to delayed pupariation time and larval lethality for *Sin<sup>GD7027</sup>* (n=180,  
1179 one-way repeat measures ANOVA with post-hoc pairwise t-test, days 6-18, p<0.05) and partial  
1180 larval lethality for *CG14182<sup>GD2738\_2</sup>* (n=120, days 7-10, p<0.05). Data represented show mean ±  
1181 standard deviation of 4-9 independent groups of 30 larvae for each line tested. **(D)** Knockdown  
1182 of 16p12.1 homologs in sensory class IV dendritic arborization neurons using *ppk-GAL4* with  
1183 overexpression of *Dicer2* showed reduced complexity of dendritic arbors (measured as sum of  
1184 intersections normalized to width) for *CG14182<sup>GD2738</sup>* (n=12, two-tailed Mann-Whitney, \*p=5.35  
1185 ×10<sup>-5</sup>). Scale bar represents 25 μm. **(E)** Third instar larvae with nervous system-specific  
1186 knockdown of 16p12.1 homologs showed reduced brain area for *CG14182<sup>GD2738\_2</sup>* (n=15, two-  
1187 tailed Mann-Whitney, \*p=0.047) and *Sin<sup>GD7027</sup>* (n=17, \*p= 0.001). **(F)** Developing third instar  
1188 larvae with knockdown of *CG14182<sup>GD2738\_2</sup>* (n=15, two-tailed Mann-Whitney, \*p=0.026) and  
1189 *Sin<sup>GD7027</sup>* (n=10, \*p= 9.74×10<sup>-4</sup>) showed reduced number of phosphorylated Histone-3 (pH3)  
1190 positive cells in the brain lobe (green). Scale bar represents 50 μm. All control data for  
1191 *Drosophila* represents phenotypes observed for the GD VDRC control (Control<sup>GD</sup>) crossed with

1192 the indicated tissue-specific *GAL4* driver. **(G)** Schematic showing the phenotypes observed with  
1193 knockdown of 16p12.1 homologs in *X. laevis*. **(H)** Representative images of tadpoles injected  
1194 with control morpholino, indicating facial landmarks for face width (yellow) and orofacial area  
1195 (red), and tadpoles with knockdown of *polr3e* and *mosmo*. Knockdown of *cdr2* (n=54, two-tailed  
1196 student's t-test,  $*p=7.75 \times 10^{-4}$ ), *polr3e* (n=37,  $*p=1.97 \times 10^{-13}$ ) and *mosmo* (n=50,  $*p=1.36 \times 10^{-11}$ )  
1197 led to decreased face width, while knockdown of *polr3e* ( $*p=3.29 \times 10^{-16}$ ) and *mosmo*  
1198 ( $*p=1.47 \times 10^{-8}$ ) led to decreased orofacial area. All measures were normalized to their respective  
1199 control injected with the same morpholino amount. Scale bar represents 500  $\mu\text{m}$ . **(I)** Strong  
1200 knockdown of *mosmo* led to decreased axon length in neural tube explants (n=566, two-tailed  
1201 student's t-test,  $*p=7.40 \times 10^{-12}$ ). All measures were normalized to their respective control  
1202 injected with the same morpholino amount. Representative schematic for axon length  
1203 measurements is shown on the left. **(J)** Representative images show forebrain (red on control  
1204 image) and midbrain (blue) areas of the side injected with morpholino (right, red asterisk), which  
1205 were normalized to the uninjected side (left). Strong knockdown of *mosmo* (n=67, two-tailed  
1206 student's t-test,  $*p<3.07 \times 10^{-13}$ ) and *polr3e* (n=48,  $*p<7.39 \times 10^{-4}$ ) led to decreased midbrain and  
1207 forebrain area of *X. laevis* tadpoles (stained with tubulin). Scale bar represents 500  $\mu\text{m}$ . In all  
1208 cases, *X. laevis* data represents strong knockdown of the 16p12.1 homologs, except for *cdr2*,  
1209 which showed lethality and is represented with partial knockdown. All control data for *X. laevis*  
1210 represents controls injected with the highest amount of morpholino (50 ng, see **S5 Fig**). Boxplots  
1211 represent all data points with median, 25th and 75th percentiles, and red dotted lines indicate the  
1212 control median. Statistical details, including sample size, confidence intervals and p-values, are  
1213 provided in **S6 File**. A list of full genotypes for fly crosses used in these experiments is provided  
1214 in **S1 File**.



1215 **Fig. 3. Homologs of 16p12.1 genes contribute both additively and interactively towards**  
1216 **neurodevelopmental defects.**

1217 (A) We generated eye-specific *GMR-GAL4* recombinant lines for the four 16p12.1 homologs to  
1218 test a total of twelve pairwise interactions for modulation of eye defects. (B) Representative  
1219 brightfield images of *Drosophila* adult eyes for recombinant lines of 16p12.1 homologs crossed  
1220 with RNAi lines for the other homologs, which show enhancement (Enh.) or suppression (Supp.)  
1221 of the phenotypes observed with crosses with control. Scale bar represents 100  $\mu$ m. (C)  
1222 Simultaneous knockdown of *UQCR-C2*<sup>GD11238</sup> with *CG14182*<sup>GD2738</sup> (n=18, two-tailed Mann-  
1223 Whitney with Benjamini-Hochberg correction, \*p=0.002) or *Sin*<sup>GD7027</sup> (n=19, \*p=0.023) led to a  
1224 significant enhancement in the eye phenotype (measured using *Flynotyper* scores) compared to  
1225 knockdown of *UQCR-C2*<sup>GD11238</sup> alone. Similarly, simultaneous knockdown of *CG14182*<sup>GD2738</sup>  
1226 with *Sin*<sup>GD7027</sup> (n=19, \*p=0.021) enhanced the eye phenotype observed for *CG14182*<sup>GD2738</sup> alone.  
1227 Simultaneous knockdown of *Cen*<sup>GD9689</sup> with *UQCR-C2*<sup>GD11238</sup> (n=20, \*p=0.023) led to a milder  
1228 suppression of the eye phenotype compared to knockdown of *Cen*<sup>GD9689</sup> alone. Double  
1229 knockdowns were compared to the recombinant lines of the 16p12.1 homologs crossed with  
1230 wild-type controls of the second 16p12.1 homolog. Note that only experiments with Control<sup>GD</sup>  
1231 are represented here; see **S8 Fig** for results from other lines with KK and BL controls. (D) We  
1232 applied a multiplicative model to identify the nature of genetic interactions for the pairwise  
1233 knockdowns tested. The expected phenotype from simultaneous knockdown of homolog A and  
1234 homolog B, or when the combined effect is additive indicating no genetic interaction (in blue),  
1235 was calculated as the product of the normalized phenotypic scores (i.e. percentage of control)  
1236 observed from knockdown of individual genes. Positive or alleviating genetic interactions were  
1237 identified for combinations where the observed phenotype was significantly milder than

1238 expected (in green), while negative or aggravating interactions were identified when the  
1239 combined phenotypes were significantly more severe than expected (in red). One-sample  
1240 Wilcoxon signed rank tests with Benjamini-Hochberg correction for multiple testing were used  
1241 to identify significant interactions. **(E)** We generated double knockdowns of 16p12.1 homologs  
1242 in *X. laevis* models by co-injecting embryos with morpholinos of two homologs. All double  
1243 knockdown experiments were performed with partial knockdown of the genes, to avoid potential  
1244 lethality with stronger knockdown. **(F)** Representative images of tadpoles stained with anti-  
1245 tubulin show forebrain (red on control image) and midbrain (blue) areas of the side injected with  
1246 morpholino (right, red asterisk), which were normalized to the uninjected side (left).  
1247 Simultaneous knockdown of *polr3e* and *mosmo* led to decreased forebrain (n=36, two-tailed  
1248 student's t-test,  $*p=1.10\times 10^{-9}$ ) and midbrain area ( $*p=1.98\times 10^{-7}$ ), which showed no differences  
1249 compared to partial knockdown of *mosmo* alone. Control data represents control injected with  
1250 highest amount of morpholino (22ng). Scale bar represents 500  $\mu\text{m}$ . **(G)** Representative western  
1251 blots show bands for phosphorylated histone-3 (pH3) and  $\beta$ -actin for the uninjected control,  
1252 knockdown of *polr3e*, knockdown of *mosmo*, and pairwise knockdown of *polr3e* and *mosmo*  
1253 (full western blots are shown in **S6 Fig**). Bar plot shows intensity of pH3 band normalized to  $\beta$ -  
1254 actin. Simultaneous knockdown of *polr3e* and *mosmo* does not lead to changes in the  
1255 proliferation defects observed with knockdown with *polr3e* alone. Boxplots represent all data  
1256 points with median, 25th and 75th percentiles, and red dotted lines indicate the control median.  
1257 Statistical details, including sample size, confidence intervals and p-values, are provided in **S6**  
1258 **File**. A list of full genotypes for fly crosses used in these experiments is provided in **S1 File**.  
1259

1260 **Fig. 4. Homologs of 16p12.1 genes show complex interactions with conserved**  
1261 **neurodevelopmental genes and homologs of patient-specific “second-hit” genes.**  
1262 (A) We evaluated how homologs of genes outside of the CNV region (*Gene B*), including genes  
1263 carrying “second-hit” variants in children with the 16p12.1 deletion, genes within conserved  
1264 neurodevelopmental pathways, and transcriptome targets, affect the phenotypes observed for  
1265 homologs of 16p12.1 genes. We crossed eye-specific recombinant lines for each homolog with a  
1266 total of 124 RNAi, mutant or overexpression lines for 76 interacting genes to test a total of 212  
1267 pairwise gene combinations. (B) Representative brightfield images of *Drosophila* adult eyes for  
1268 recombinant lines of 16p12.1 homologs crossed with background-specific controls (Control<sup>KK</sup>,,  
1269 also represented as C<sup>KK</sup>) or RNAi lines for *kis* and *CG10465*, are shown as examples of genetic  
1270 interactions between the 16p12.1 homologs and homologs of neurodevelopmental genes. Bar  
1271 plots show normalized phenotypes (median  $\pm$  interquartile range) for 16p12.1 recombinant lines  
1272 crossed with background-specific control or with RNAi lines for interacting genes. *Sin*<sup>GD7027</sup>  
1273 negatively interacted with *kis*<sup>KK100890</sup> and led to a more severe phenotype (two-tail one-sample  
1274 Wilcoxon signed rank test with Benjamini-Hochberg correction, n=11, \*p=0.012, in red) than  
1275 expected (in blue) under a multiplicative model. Similarly, *CG10465*<sup>KK105756</sup> negatively  
1276 interacted with *UQCR-C2*<sup>GD11238</sup> (n=10, \*p=0.024) and *CG14182*<sup>GD2738</sup> (n=10, \*p=0.015),  
1277 leading to more severe eye phenotypes than expected. Phenotypes are represented as percentage  
1278 of average, i.e. normalized to *Flynotyper* scores from control flies carrying the same genetic  
1279 background as the interacting gene. Scale bar represents 100  $\mu$ m. (C) Heatmaps show interaction  
1280 scores calculated as the log<sub>2</sub> ratio between the average of observed and expected phenotypic  
1281 scores. Positive scores represent negative aggravating genetic interactions (in red), while  
1282 negative scores represent positive alleviating interactions (in green). Grey boxes indicate

1283 pairwise crosses that were not tested or were not validated by multiple lines. A complete list of  
1284 interaction scores is provided in **S4 File. (D)** Scatter plots depict interactions tested for 16p12.1  
1285 homologs. The plots show the average phenotypic score of the interacting gene on the x-axis,  
1286 and the average observed phenotypic score for the pairwise knockdown on the y-axis. The blue  
1287 line represents the expected phenotypic score of the pairwise knockdown calculated for each  
1288 16p12.1 homolog (value of first hit crossed with control, such as  $UQCR-C2^{GD11238}$  X Control<sup>BL</sup>),  
1289 and all possible phenotypic scores (ranging from 0 to 60) of the interacting genes are represented  
1290 on the x-axis. All positive and negative (validated or potential) interactions are represented in  
1291 green and red, respectively, and fly lines of genes with no significant interactions are shown in  
1292 grey. Only lines from the BDSC stock center are represented here; **S17 Fig.** shows scatter plots  
1293 representing VDRC stock lines.

1294

1295 **Fig. 5. Homologs of patient-specific “second-hits” modulate phenotypes of 16p12.1**  
1296 **homologs through additive and interactive effects.**

1297 **(A)** Representative pedigrees of families with 16p12.1 deletion (affected child in black, carrier  
1298 parent in grey) that were selected to study the effect of homologs (represented within  
1299 parenthesis) of genes carrying “second-hits” towards phenotypes of homologs of 16p12.1 genes.  
1300 **(B)** Plots show the changes in *Flynotyper* scores (mean  $\pm$  s.d.) for *GMR-GAL4* control (grey) or  
1301 recombinant lines of 16p12.1 homologs crossed with either background-specific control line  
1302 (left) or with “second-hit” homologs (right). We note that represented changes in *Flynotyper*  
1303 scores for  $Cen^{GD9689}/NrX-1^{GD14451\_2}$ ,  $UQCR-C2^{GD11238}/Zasp52^{HMJ22168}$ , and  
1304  $Sin^{GD7027}/Zasp52^{HMJ22168}$  were not validated with multiple RNAi lines for the “second-hit”  
1305 homolog. *Flynotyper* values for all the tested pairwise knockdowns are shown in **S11-S14 Fig**

1306 and validated enhancements and suppressions (using Mann-Whitney tests) are shown in **S15-S16**  
1307 **Fig. (C)** Representative brightfield adult eye images for pairwise knockdowns that enhanced  
1308 (Enh.) or suppressed (Supp.) phenotypes of 16p12.1 homologs are shown. Scale bar represents  
1309 100  $\mu\text{m}$ . **(D)** Bar plots show normalized phenotypes (median  $\pm$  interquartile range) for the  
1310 16p12.1 recombinant lines crossed with background-specific controls (Control<sup>GD</sup> or Control<sup>BL</sup>,  
1311 also represented as C<sup>GD</sup>, C<sup>BL</sup>, respectively) or with RNAi lines for *Nrx-1*<sup>GD14451-2</sup>,  
1312 *Cep135*<sup>GD6121-2</sup>, *Zasp52*<sup>HMJ22168</sup>, *shot*<sup>HMJ23381</sup>, *Rpn2*<sup>HMS0533</sup>, *Dhc98*<sup>DMB03402</sup>, as examples of genetic  
1313 interactions identified between the 16p12.1 homologs and homologs of patient-specific “second-  
1314 hit” genes. *Sin*<sup>GD7027</sup> negatively interacted with *Cep135*<sup>GD6121-2</sup> and led to a more aggravating  
1315 phenotype (two-tail one-sample Wilcoxon signed rank test with Benjamini-Hochberg correction,  
1316 n=10, \*p=0.012, in red) than expected (in blue) under a multiplicative model, while other  
1317 examples of pairwise knockdowns with homologs “second-hit” genes shown here led to positive  
1318 genetic interactions (\*p<0.05, in green). Details of number of homologs, fly lines and crosses, as  
1319 well as a list of full genotypes for all interaction experiments are provided in **S1 File**. Statistical  
1320 details, including sample size, confidence intervals, and p-values, are provided in **S6 File**.

1321

1322 **Fig. 6. Homolog of *SETD5* synergistically interact with homologs of *MOSMO* to modify**  
1323 **neurodevelopmental defects.**

1324 **(A)** Pedigree of a family with 16p12.1 deletion, with the proband also carrying a *de novo*  
1325 pathogenic mutation in *SETD5*. Representative brightfield adult eye images for control and  
1326 *GMR-GAL4* knockdown of *CG14182*<sup>GD2738</sup>, *upSET*<sup>HMC03177</sup>, and *CG14182*<sup>GD2738</sup>/*upSET*<sup>HMC03177</sup>  
1327 are shown. Data show a negative genetic interaction with simultaneous knockdown of  
1328 *CG14182*<sup>GD2738</sup> and *upSET*<sup>HMC03177</sup>. Bar plots show normalized phenotypes (median  $\pm$

1329 interquartile range) for recombinant lines of *CG14182*<sup>GD2738</sup> and *Sin*<sup>GD7027</sup> crossed with  
1330 background-specific control (Control<sup>BL</sup>, also represented as C<sup>BL</sup>) or *upSET*<sup>HMC03177</sup>. An  
1331 aggravating phenotype is observed with *CG14182*<sup>GD2738</sup>/*upSET*<sup>HMC03177</sup> (two-tailed one-sample  
1332 Wilcoxon signed rank test with Benjamini-Hochberg correction, n=9, \*p=0.018, in red) than  
1333 expected (in blue). **(B)** Representative confocal images of third instar larval eye discs stained  
1334 with anti-phosphorylated histone-3 (pH3, green) or anti-Dcp-1 (red), markers of cellular  
1335 proliferation and apoptosis, respectively. Positive pH3 or Dcp-1 cells were quantified posterior to  
1336 the morphogenetic furrow, indicated by white boxes in left panels. Double knockdown of  
1337 *CG14182*<sup>GD2738</sup>/*upSET*<sup>HMC03177</sup> led to increased pH3 (n=17, two-tailed Mann-Whitney, \*p=  
1338 0.046) and Dcp-1 (n=19, \*p=0.006) positive cells compared to knockdown of *CG14182*<sup>GD2738</sup>  
1339 alone. The double knockdown also led to increased Dcp-1 positive cells compared to knockdown  
1340 of *upSET*<sup>HMC03177</sup> alone (\*p= 2.19×10<sup>5</sup>). Scale bar represents 50 μm. **(C)** Representative images  
1341 of tadpoles stained with anti-tubulin show forebrain (red on control image) and midbrain (blue)  
1342 areas of the side injected with morpholino (right, red asterisk), which were normalized to the  
1343 uninjected side (left). Partial knockdown of *mosmo* with *setd5* led to a reduction in the midbrain  
1344 area compared to the knockdown of *mosmo* alone (n=16, two-tailed student's t-test, \*p= 0.047).  
1345 Control data represents control injected with highest amount of morpholino (22ng). Scale bar  
1346 represents 500 μm **(D)** Normalized axon length of *X. laevis* tadpoles with simultaneous  
1347 knockdown of *mosmo* and *setd5* led to a significant reduction in axon length that was not  
1348 observed with partial knockdown of *mosmo* (n=438, two-tailed student's t-test, \*p= 3.34 ×10<sup>-6</sup>)  
1349 or *setd5* (\*p=1.86 ×10<sup>-9</sup>). All measures were normalized to their respective controls injected with  
1350 the same morpholino amount (See **S20 Fig**). Control data represents controls injected with  
1351 highest amount of morpholino (22ng). All double knockdown experiments were performed with

1352 partial knockdown of the genes, to avoid potential lethality with stronger knockdown. Boxplots  
1353 represent all data points with median, 25th and 75th percentiles, and red dotted lines indicate the  
1354 control median. A list of full genotypes for fly crosses used in these experiments is provided in  
1355 **S1 File**. Statistical details, including sample size, confidence intervals and p-values, are provided  
1356 in **S6 File**.

1357

1358 **Fig. 7. Functional relatedness of genes within disease-associated CNV regions correspond**  
1359 **with higher pathogenicity.**

1360 (A) Bar plot shows frequency of reported *de novo* occurrence of the 16p12.1 deletion (9, 11)  
1361 compared to the autism-associated 16p11.2 deletion (11, 105, 106). Schematic shows a model for  
1362 higher functional connectivity of genes within the 16p11.2 region compared to the 16p12.1  
1363 region. Only genes with *Drosophila* homologs are represented. (B) Phenotypic scores of  
1364 individual 16p11.2 homologs (grey) are significantly enhanced or suppressed by a second  
1365 16p11.2 homolog (orange). In contrast, little variation in phenotypic scores is observed for  
1366 16p12.1 homologs (grey) with simultaneous knockdown of another homolog (green). The  
1367 interacting homologs are labeled as follows: A: *Pp4-19C (PPP4C)*, B: *CG17841 (FAM57B)*, C:  
1368 *coro (CORO1A)*, D: *Ald1 (ALDOA)*, E: *Rph (DOC2A)*, F: *Tao (TAOK2)*, G: *Asph (ASPHD1)*, H:  
1369 *kfp68D (KIF22)*, I: *Pal (PAGR1)*, J: *Pis (CDIPT)*, K: *CG10465 (KCTD13)*, L: *CG15309*  
1370 *(YPEL3)*, M: *Doc3, (TBX6)*, N: *rl (MAPK3)*, W: *CG14182 (MOSMO)*, X: *Cen (CDR2)*, Y: *Sin*  
1371 *(POLR3E)*, Z: *UQCR-C2 (UQCRC2)*. (C) Pairwise knockdown of homologs of 16p11.2 genes  
1372 (n=27) show a larger magnitude of interactions compared with those among 16p12.1 homologs  
1373 (n=5, two-tailed Mann-Whitney test, \*p=0.011). Interaction values of zero (blue shade) represent  
1374 no interactions or additive effects, while values above or below zero represent negative (in red)

1375 and positive (in green) interactions, respectively. **(D)** Pairs of 16p11.2 homologs exhibit a higher  
1376 proportion of shared differentially-expressed genes compared to pairs of 16p12.1 homologs  
1377 (n=30 for 16p11.2, n=12 for 16p12.1, two-tailed Mann-Whitney test, \*p= 0.031). **(E)** Network  
1378 diagram shows connections between human 16p11.2 or 16p12.1 genes within a brain-specific  
1379 interaction network. 16p12.1 genes are indicated in green, 16p11.2 genes in orange, connector  
1380 genes in grey, and connector genes that are intolerant to functional variation (RVIS  $\leq$  20<sup>th</sup>  
1381 percentile) in dark green. *C16orf92* and *C16orf54* for 16p11.2 and *PDZD9* for 16p12.1 were not  
1382 present in the brain network and were therefore excluded from the network analysis. **(F)** Genes  
1383 within the 16p11.2 region show higher average pairwise connectivity in a human brain-specific  
1384 network, measured as the inverse of the shortest paths between two genes, compared to 16p12.1  
1385 genes (n=25 for 16p11.2, n=6 for 16p12.1, two-tailed Mann-Whitney, \*p=0.036, see **S5 File**).  
1386 **(G)** 16p11.2 connector genes have lower RVIS percentile scores compared to 16p12.1 connector  
1387 genes (n=166 for 16p11.2, n=33 for 16p12.1, two-tailed Mann-Whitney, \*p=0.017, see **S5 File**).  
1388 Functionally-intolerant genes are represented in dark green. Boxplots represent all data points  
1389 with median, 25th and 75th percentiles. Statistical details are provided in **S6 File**.  
1390



## 1391 **Supporting Information Legends**

### 1392 **S1 Fig. Expression levels of 16p12.1 homologs in *Drosophila* and *X. laevis*.**

1393 **(A)** *Drosophila* homologs of 16p12.1 genes were knocked down using nervous system-specific  
1394 *Elav-GAL4* driver with overexpression of *Dicer2* at 25°C. RT-qPCR confirmed 40-60%  
1395 knockdown of the 16p12.1 homologs (two-tailed student's t-test, \* $p < 0.05$ ). As knockdown of *Sin*  
1396 caused embryonic lethality in these conditions, all experiments in the nervous system and RT-  
1397 qPCR were performed without overexpression of *Dicer2* and reared at room temperature (RT).  
1398 *Sin*<sup>KK101936</sup> and *Sin*<sup>HMC03807</sup> were also embryonic lethal without *Dicer2*. *Sin*<sup>GD7027\_2</sup> did not show  
1399 knockdown of the homolog, and the RNAi line was therefore not used for further experiments.  
1400 All experiments were performed in comparison to appropriate background-specific controls.  
1401 Only one control is shown per gene. GD VDRC Control is shown in all cases for simplification  
1402 (Control<sup>GD</sup>). A list of full genotypes for fly crosses used in these experiments is provided in **S1**  
1403 **File.** **(B)** Normalized band intensity of RT-PCR of *X. laevis* tadpoles injected with different  
1404 morpholino dosages of the 16p12.1 homologs compared to the uninjected control. Different  
1405 morpholino sequences were used for the L and S alleles for *uqcrc2* and *mosmo*, while unique  
1406 sequences were used for both L and S alleles for *cdr2* or *setd5*. As the S allele has not been  
1407 annotated for *polr3e*, only the L allele was targeted. Colored bars represent the dosages of  
1408 morpholinos used, with grey bars indicating amounts for “partial knockdown” (approximately  
1409 50% of expression) and black bars indicating amounts for “stronger knockdown”. 10ng of  
1410 morpholino was used for partial and stronger KD experiments for *mosmo* S allele, as increasing  
1411 concentrations did not lead to differences in knockdown of the allele. Bar plots represent mean  
1412 +/- SD, and red dotted lines indicate 50% expression. Statistical details are provided in **S6 File**.

1413

1414 **S2 Fig. Global neurodevelopmental defects with knockdown of 16p12.1 *Drosophila***

1415 **homologs.**

1416 (A) Summary of phenotypes observed with tissue-specific knockdown of each of the 16p12.1

1417 homologs. (B) Ubiquitous (*Da-GAL4*) and nervous system-specific (*Elav-GAL4*) knockdown of

1418 multiple RNAi lines for each 16p12.1 homolog showed a range of lethality and developmental

1419 defects. (C) Representative brightfield images of adult wings with knockdown of 16p12.1

1420 homologs using the wing-specific driver *bx<sup>MS1096</sup>-GAL4*. Severe phenotypes were observed for

1421 *UQCR-C2* and *Sin*, with some RNAi lines, including *UQCR-C2<sup>GD11238\_2</sup>*, *UQCR-C2<sup>KK108812</sup>* and

1422 *Sin<sup>GD7027</sup>*, showing lethality. Scale bar represents 500µm. (D) Bang sensitivity assay for adult

1423 flies with nervous system-specific knockdown of the 16p12.1 homologs showed increased

1424 recovery time for *UQCR-C2<sup>GD11238</sup>* (n=95, two-tailed Mann-Whitney test, \*p=0.003). *Sin<sup>GD7027</sup>*

1425 adult flies exhibited severe motor defects and could not be tested for the phenotype. Boxplots

1426 represent all data points with median, 25th and 75th percentiles. Statistical details are provided in

1427 **S6 File**. A list of full genotypes for fly crosses used in these experiments is provided in **S1 File**.

1428

1429 **S3 Fig. *Sin<sup>GD7027</sup>* and *CGI4182<sup>GD2738\_2</sup>* lead to decreased brain area and decreased number**

1430 **of proliferating cells in the brain.**

1431 (A) Representative confocal brightfield images of nervous system-specific knockdown of

1432 16p12.1 homologs show decreased total brain area for *Sin<sup>GD7027</sup>* and *CGI4182<sup>GD2738\_2</sup>*. Scale bars

1433 represent 100µm. (B) *Elav-GAL4* mediated knockdown led to decreased number of

1434 phosphorylated histone-3 positive cells (pH3, green) in the brain lobe (DAPI, blue) with

1435 knockdown of *Sin<sup>GD7027</sup>* (n=10, two-tailed Mann-Whitney, \*p= 9.74×10<sup>-4</sup>) and *CGI4182<sup>GD2738\_2</sup>*

1436 (n=15, \*p=0.026), indicating decreased proliferation with knockdown of the homologs.

1437 Knockdown of *Sin*<sup>GD7027</sup> led to decreased number of Dcp-1 positive cells (\*p= 2.78×10<sup>-4</sup>, red) in  
1438 the brain lobe. Scale bar represents 50µm. Boxplots represent all data points with median, 25th  
1439 and 75th percentiles. Statistical details, including sample size, confidence intervals and p-values,  
1440 are provided in **S6 File**. A list of full genotypes for fly crosses used in these experiments is  
1441 provided in **S1 File**.

1442

1443 **S4 Fig. Enriched GO terms observed with knockdown of 16p12.1 fly homologs in the**  
1444 **nervous system.**

1445 (A) Clusters of enriched Gene Ontology (GO) Biological Process terms for differentially  
1446 expressed fly genes observed with nervous system-specific knockdown of 16p12.1 homologs  
1447 (left) and their human homologs (right). While some clusters of terms overlap among 16p12.1  
1448 homologs, genes dysregulated with knockdown of individual homologs exhibit unique  
1449 enrichments for GO terms, suggesting their independent action towards neuronal development.  
1450 Venn diagrams show overlaps of enriched GO Complete Biological Processes terms for (B)  
1451 differentially-expressed fly genes observed with knockdown of individual 16p12.1 homologs, or  
1452 (C) human homologs of the fly genes. We also observed that most of the (D) fly homologs or (E)  
1453 human counterparts of the differentially-expressed genes were unique to each 16p12.1 homolog.  
1454 A list of differentially expressed genes with knockdown of 16p12.1 homologs, as well as a list of  
1455 all enriched GO terms for these gene sets, is detailed in **S2 File**. Venn diagrams were constructed  
1456 using Venny 2.1 software (<https://bioinfogp.cnb.csic.es/tools/venny>).

1457

1458 **S5 Fig. Decreased dosage of 16p12.1 homologs leads to multiple neurodevelopmental**  
1459 **phenotypes in *X. laevis*.**

1460 **(A)** Representative images of tadpoles injected with control morpholino or morpholinos for  
1461 16p12.1 homologs, indicating facial landmarks for face width (yellow), height (blue), angle  
1462 (green), and orofacial (red) and eye (orange) area. Boxplots showing face height, width, angle,  
1463 and orofacial and eye area of each knockdown compared to its own control. Knockdown of  
1464 *mosmo* (n=50, two-tailed student's t-test, \*p=0.010) and *cdr2* (n=54, \*p=3.68×10<sup>-6</sup>) led to  
1465 increased face height. Knockdown of *cdr2* (\*p=7.75 ×10<sup>-4</sup>), *polr3e* (n=37, \*p=1.97 ×10<sup>-13</sup>) and  
1466 *mosmo* (\*p=1.36 ×10<sup>-11</sup>) led to decreased face width, while knockdown of *cdr2* (\*p= 1.03×10<sup>-8</sup>),  
1467 *polr3e* (\*p= 2.73×10<sup>-4</sup>) and *mosmo* (\*p= 3.50×10<sup>-7</sup>) led to decreased face angle. Knockdown of  
1468 *polr3e* (\*p=3.29 ×10<sup>-16</sup>) and *mosmo* (\*p=1.47 ×10<sup>-8</sup>) led to decreased orofacial area, and  
1469 knockdown of *polr3e* (\*p=1.01×10<sup>-18</sup>), *mosmo* (\*p= 7.23×10<sup>-10</sup>) and *cdr2* (\*p= 0.009) led to  
1470 decreased eye area. Data represents strong knockdown of the 16p12.1 homologs, except for *cdr2*,  
1471 which showed lethality and is represented with partial knockdown. All measures were  
1472 normalized to their respective control injected with the same morpholino amount. Scale bars  
1473 represent 500µm. **(B)** Boxplots showing axon length of each knockdown compared to its own  
1474 control. Strong knockdown of *mosmo* led to decreased axon length in neural tube explants  
1475 (n=548, two-tailed student's t-test, \*p=7.40 ×10<sup>-12</sup>), which was rescued by co-injection with  
1476 overexpressed (OE) mRNA of the gene (n=566, \*p= 4.06×10<sup>-5</sup>). All measures were normalized  
1477 to their respective control injected with the same morpholino amount. **(C)** Representative images  
1478 stained with anti-tubulin show forebrain (red on control image) and midbrain (blue) areas of the  
1479 side injected with morpholino (right, red asterisk), which were normalized to the uninjected side  
1480 (left). Partial knockdown of *mosmo* led to decreased forebrain (n=47, two tailed student's t-test,  
1481 \*p= 1.18×10<sup>-9</sup>) and midbrain (\*p=1.45×10<sup>-7</sup>) area. Graphs represent contralateral ratio of brain  
1482 area compared to uninjected side of the embryo. Scale bars represent 500µm. All boxplots

1483 represent all data points with median, 25th and 75th percentiles. In each case, measurements for  
1484 each knockdown were compared to controls injected with equal amounts of morpholino.  
1485 Statistical details, including sample size, confidence intervals and p-values, are provided in **S6**  
1486 **File**.

1487

1488 **S6 Fig. Whole western blot for phosphorylated histone-3 in *X. laevis* embryos with**  
1489 **knockdown of *polr3e*, *mosmo* and *setd5*.**

1490 (A) Three replicate western blot experiments were performed. The intensity of bands at 17 kDa,  
1491 corresponding with pH3 (top, indicated with arrow), were normalized to the  $\beta$ -actin loading  
1492 control (bottom). (B) Partial knockdown of *polr3e* shows reduced band intensity with anti-pH3  
1493 antibody compared to  $\beta$ -actin loading control. Bar plot represents mean  $\pm$  SD.

1494

1495 **S7 Fig. Knockdown of *Sin* and *CG14182* lead to disruption of the fly eye in a dosage**  
1496 **sensitive manner.**

1497 (A) Representative brightfield adult eye images and *Flynotyper* phenotypic scores of eye-specific  
1498 knockdown of 16p12.1 homologs with *GMR-GAL4* and no overexpression of *Dicer2* at 30°C. A  
1499 mild eye phenotype was observed with knockdown of *Sin*, replicated across multiple RNAi lines  
1500 (two-tailed Mann-Whitney with Benjamini-Hochberg correction, \* $p < 0.05$ ). (B) Representative  
1501 images and *Flynotyper* scores of eye-specific knockdown of 16p12.1 homologs with *GMR-GAL4*  
1502 and overexpression of *Dicer2* at 30°C. Severe eye phenotypes were observed for all tested RNAi  
1503 lines of *Sin* (\* $p < 1.13 \times 10^{-4}$ ) and *CG14182* (\* $p < 4.70 \times 10^{-4}$ ). Scale bar represents 100  $\mu$ m.

1504 Boxplots represent all data points with median, 25th and 75th percentiles, and red dotted lines  
1505 indicate the control median. Statistical details, including sample size, confidence intervals and p-

1506 values, are provided in **S6 File**. A list of full genotypes for fly crosses used in these experiments  
1507 is provided in **S1 File**.

1508

1509 **S8 Fig. Pairwise knockdown of homologs of 16p12.1 genes lead to moderate changes in eye**  
1510 **severity compared to individual knockdown of genes.**

1511 **(A-D)** Pairwise knockdown of homologs of 16p12.1 genes led to subtle changes in phenotypic  
1512 scores, with only four significant interactions (compared to control lines) validated by multiple  
1513 RNAi lines. *Sin* and *CG14182* enhanced the eye phenotype of *UQCR-C2*<sup>GD11238</sup>, while *Sin*  
1514 enhanced *CG14182*<sup>GD2738</sup> eye phenotype and *UQCR-C2* suppressed *Cen*<sup>GD9689</sup> eye phenotype  
1515 (two-tailed Mann-Whitney with Benjamini-Hochberg correction, \*p<0.05). Boxplots represent  
1516 all data points with median, 25th and 75th percentiles. Red dotted lines indicate the median of  
1517 recombinant lines crossed with control. Statistical details, including sample size, confidence  
1518 intervals and p-values, are provided in **S6 File**. A list of full genotypes for fly crosses used in  
1519 these experiments is provided in **S1 File**.

1520

1521 **S9 Fig. Range of observed and expected phenotypic scores using a multiplicative model.**

1522 Histograms representing the distribution of observed (in grey) and expected (in blue) phenotypic  
1523 scores of *GMR-GAL4*-mediated pairwise knockdowns of 16p12.1 homologs and interacting  
1524 genes (top panel) and *GMR-GAL4*-mediated single knockdowns of potential interacting genes  
1525 tested (bottom panel). The distribution shows an overlap of the observed and expected  
1526 phenotypic scores values.

1527

1528 **S10 Fig. Expected genetic interactions for each category of interacting gene analyzed in this**  
1529 **study.** The diagram shows representative gene networks of each of the 16p12.1 homologs  
1530 analyzed. *UQCR-C2* is shown as an example, where the gene is closely connected to  
1531 transcriptome targets and functionally related genes, while neurodevelopmental genes and  
1532 patient-specific “second-hit” genes distribute more randomly between gene categories that can  
1533 lead to positive and negative genetic interactions (top bubble) or additive effects (bottom  
1534 bubble). These hypotheses aligned with our results, as we identified genetic interactions for  
1535 42/61 pairwise combinations (68.8%) with direct transcriptome targets, compared to 22/55  
1536 (40%) interactions identified with functionally related and neurodevelopmental genes ( $p=0.0027$ ,  
1537 Fisher’s exact test). Moreover, we observed that homologs of genes carrying “second-hits” in  
1538 severely affected children with the 16p12.1 deletion interacted with 16p12.1 homologs in 37/96  
1539 (38.5%) of the pairs, although the proportion of genetic interactions was not as high compared to  
1540 that identified with functionally related genes or genes in neurodevelopmental pathways and  
1541 transcriptome targets (64/101, 63%, Fisher’s exact test,  $p=0.019$ ).

1542

1543 **S11 Fig. Phenotypic scores of the tested pairwise interactions of *UQCR-C2*<sup>GD11238</sup> with**  
1544 **homologs of “second-hit” or neurodevelopmental genes in *Drosophila* eye.**

1545 *Flynotyper* phenotypic scores of *UQCR-C2*<sup>GD11238</sup> crossed with RNAi, mutant or overexpression  
1546 lines of (A) neurodevelopmental genes or genes functionally related with *UQCR-C2* function, (B  
1547 and C) homologs of “second-hits” identified in children with 16p12.1 deletion, and (D)  
1548 transcriptome targets and functionally related groups identified in RNA-sequencing of *UQCR-C2*  
1549 knockdown model. Boxplots represent all data points with median, 25th and 75th percentiles.  
1550 Red dotted lines indicate the median of recombinant lines crossed with control. A list of full

1551 genotypes and statistics, including sample size, confidence intervals and p-values, for these  
1552 experiments are provided in **S1 File** and **S6 File**.

1553

1554 **S12 Fig. Phenotypic scores of the tested pairwise interactions of *Cen*<sup>GD9689</sup> with homologs of**  
1555 **“second-hit” or neurodevelopmental genes in *Drosophila* eye.**

1556 *Flynotyper* phenotypic scores of *Cen*<sup>GD9689</sup> crossed with RNAi, mutant or overexpression lines of  
1557 (A) neurodevelopmental genes or genes functionally related with *Cen* function, (B and C)  
1558 homologs of “second-hits” identified in children with 16p12.1 deletion, and (D) transcriptome  
1559 targets and functionally related groups identified in RNA-sequencing of *Cen* knockdown model.  
1560 Boxplots represent all data points with median, 25th and 75th percentiles. Red dotted lines  
1561 indicate the median of recombinant lines crossed with control. A list of full genotypes and  
1562 statistics, including sample size, confidence intervals, and p-values, for these experiments are  
1563 provided in **S1 File** and **S6 File**.

1564

1565 **S13 Fig. Phenotypic scores of the tested pairwise interactions of *Sin*<sup>GD7027</sup> with homologs of**  
1566 **“second-hit” or neurodevelopmental genes in *Drosophila* eye.**

1567 *Flynotyper* phenotypic scores of *Sin*<sup>GD7027</sup> crossed with RNAi, mutant or overexpression lines of  
1568 (A) neurodevelopmental genes or genes functionally related with *Sin* function, (B and C)  
1569 homologs of “second-hits” identified in children with 16p12.1 deletion, and (D and E)  
1570 transcriptome targets and functionally related groups identified in RNA-sequencing of *Sin*  
1571 knockdown model. Boxplots represent all data points with median, 25th and 75th percentiles.  
1572 Red dotted lines indicate the median of recombinant lines crossed with control. A list of full



1573 genotypes and statistics, including sample size, confidence intervals and p-values, for these  
1574 experiments are provided in **S1 File** and **S6 File**.

1575

1576 **S14 Fig. Phenotypic scores of the tested pairwise interactions of *CG14182*<sup>GD2738</sup> with**  
1577 **homologs of “second-hit” or neurodevelopmental genes in *Drosophila* eye.**

1578 *Flyntyper* phenotypic scores of *CG14182*<sup>GD2738</sup> crossed with RNAi, mutant or overexpression  
1579 lines of (A) neurodevelopmental genes or genes functionally related with *CG14182* function, (B  
1580 and C) homologs of “second-hits” identified in children with 16p12.1 deletion, and (D)  
1581 transcriptome targets and functionally related groups identified in RNA-sequencing of *CG14182*  
1582 knockdown model. Boxplots represent all data points with median, 25th and 75th percentiles.  
1583 Red dotted lines indicate the median of recombinant lines crossed with control. A list of full  
1584 genotypes and statistics, including sample size, confidence intervals and p-values, for these  
1585 experiments are provided in **S1 File** and **S6 File**.

1586

1587 **S15 Fig. Multiple homologs of patient-specific “second-hits” and neurodevelopmental genes**  
1588 **modulate phenotypes caused by knockdown of *UQCR-C2*<sup>GD11238</sup> and *Cen*<sup>GD9689</sup>.**

1589 Representative brightfield adult eye images and phenotypic scores of eyes from RNAi, mutant or  
1590 overexpression lines of neurodevelopmental genes, homologs of genes with “second-hits” in  
1591 children with 16p12.1 deletion, and transcriptome targets that significantly enhanced (Enh.) or  
1592 suppressed (Supp.) the phenotypes of recombinant lines of *UQCR-C2*<sup>GD11238</sup> (A) or *Cen*<sup>GD9689</sup> (B)  
1593 (\*p<0.05, two-tailed Mann-Whitney tests with Benjamini-Hochberg correction). Scale bar  
1594 represents 100 μm. Boxplots represent all data points with median, 25th and 75th percentiles.

1595 Red dotted lines indicate the median of recombinant lines crossed with control. A list of full  
1596 genotypes and statistics, including sample size, confidence intervals and p-values, for these  
1597 experiments are provided in **S1 File** and **S6 File**.

1598

1599 **S16 Fig. Multiple homologs of patient-specific “second-hits” and neurodevelopmental genes**  
1600 **modulate phenotypes caused by knockdown of *CG14182*<sup>GD2738</sup> and *Sin*<sup>GD7027</sup>.**

1601 Representative brightfield adult eye images and phenotypic scores of eyes from RNAi, mutant or  
1602 overexpression lines of neurodevelopmental genes, homologs of genes with “second-hits” in  
1603 children with 16p12.1 deletion, and transcriptome targets that significantly enhanced (Enh.) or  
1604 suppressed (Supp.) the phenotypes of recombinant lines of *CG14182*<sup>GD2738</sup> (**A**) or *Sin*<sup>GD7027</sup> (**B**)  
1605 (\*p<0.05, two-tailed Mann-Whitney tests with Benjamini-Hochberg correction). Scale bar  
1606 represents 100  $\mu$ m. Boxplots represent all data points with median, 25th and 75th percentiles.  
1607 Red dotted lines indicate the median of recombinant lines crossed with control. A list of full  
1608 genotypes and statistics, including sample size, confidence intervals and p-values, for these  
1609 experiments are provided in **S1 File** and **S6 File**.

1610

1611 **S17 Fig. Genetic interactions between 16p12.1 homologs and neurodevelopmental genes,**  
1612 **transcriptome targets and homologs of patient-specific “second-hit” genes.** Scatter plots  
1613 depict the interactions tested for *GMR-GAL4* recombinant lines for *UQCR-C2*<sup>GD11238</sup> (**A**),  
1614 *Cen*<sup>GD9689</sup> (**B**), *CG14182*<sup>GD2738</sup> (**C**), and *Sin*<sup>GD7027</sup> (**D**). The plots show the average phenotypic  
1615 score of the interacting gene on the x-axis using VDRC GD (top) or KK (bottom) fly lines and  
1616 the average observed phenotypic score for the double knockdown on the y-axis. Blue line  
1617 represents the expected phenotypic score of the pairwise knockdown calculated as the product of

1618 the first hit phenotype (*Flyntyper* score of first hit crossed with control, such as *UQCR-*  
1619 *C2<sup>GD11238</sup>* X Control<sup>GD</sup>) for each theoretical phenotypic value of interacting gene (ranging from 0  
1620 to 60) represented on x-axis. All positive and negative (validated or potential) interactions are  
1621 represented in green and red, respectively, and fly lines of genes with no significant interactions  
1622 are shown in grey.

1623

1624 **S18 Fig. “Second-hit” genes identified in probands with 16p12.1 deletion.**

1625 Pedigrees of 15 families with the 16p12.1 deletion, highlighting 23 genes with rare secondary  
1626 likely-pathogenic mutations (CNVs and SNVs) that were identified in severely affected children  
1627 with the 16p12.1 deletion. These 23 genes carrying “second-hit” mutations were selected for  
1628 *Drosophila* experiments to test how their decreased expression affects the neurodevelopmental  
1629 phenotypes observed for 16p12.1 homologs. Family members who carry either the 16p12.1  
1630 deletion or individual genes with “second-hits” are indicated in the pedigrees. Phenotypes  
1631 observed for affected children and other family members are indicated below each pedigree.

1632

1633 **S19 Fig. *Osa* and *Nipped-A* interact with *CG14182<sup>GD2738</sup>* through cellular processes during**  
1634 **eye development.**

1635 (A) Representative brightfield adult eye images show that simultaneous knockdown of  
1636 *CG14182<sup>GD2738</sup>* with *osa<sup>JF01207</sup>* leads to a suppressed (Supp.) eye phenotype, while simultaneous  
1637 knockdown of *Nipped-A<sup>HMS00167</sup>* leads to synergistic enhancement (Enh.) in eye phenotype  
1638 compared to single knockdown of *CG14182<sup>GD2738</sup>*. Scale bar represents 100  $\mu$ m. (B)

1639 Representative confocal images of third instar larval eye discs stained with DAPI (blue) and anti-  
1640 phosphorylated histone-3 (pH3, green) or anti-Dcp-1 (red), markers of cellular proliferation and

1641 apoptosis, respectively. Positive pH3 or Dcp-1 cells were quantified posterior to the  
1642 morphogenetic furrow (indicated by white boxes). Simultaneous knockdown of *CG14182*<sup>GD2738</sup>  
1643 with *osa*<sup>JF01207</sup> led to an increase in the number of pH3 positive cells (n=20, two-tailed Mann-  
1644 Whitney, \*p= 2.33×10<sup>-6</sup>) compared to the single knockdown of *CG14182*<sup>GD2738</sup>. (C)  
1645 Simultaneous knockdown of *CG14182*<sup>GD2738</sup> with *Nipped-A*<sup>HMS00167</sup> led to a significant reduction  
1646 in the number of Dcp-1 positive cells compared to single knockdown of *CG14182*<sup>GD2738</sup> (n=15,  
1647 in red, two-tailed, Mann-Whitney, \*p=2.54×10<sup>-5</sup>). Scale bars represent 50 μm. Boxplots  
1648 represent all data points with median, 25th and 75th percentiles. Statistical details, including  
1649 sample size, confidence intervals and p-values, are provided in **S6 File**. A list of full genotypes  
1650 for fly crosses used in these experiments is provided in **S1 File**.

1651

1652 **S20 Fig. *setd5* modifies phenotypes observed with knockdown of *polr3e* and *mosmo* in *X.***  
1653 ***laevis*.**

1654 (A) Representative images stained with anti-tubulin show forebrain (red on control image) and  
1655 midbrain (blue) areas of the side injected with morpholino (right, red asterisk), normalized to the  
1656 uninjected side (left). Simultaneous knockdown of *polr3e* and *setd5* in *X. laevis* led to decreased  
1657 forebrain (n=28, two-tailed student's t-test, \*p=6.01×10<sup>-7</sup>) and midbrain area (\*p=1.67×10<sup>-7</sup>)  
1658 compared to knockdown of *polr3e* alone, which were not different to the partial knockdown of  
1659 *setd5* alone (p>0.05). Scale bar represents 500 μm. (B) Normalized axon length of *X. laevis*  
1660 tadpoles with simultaneous knockdown of *mosmo* and *setd5* showed decreased axon length  
1661 different from the control injected with 22ng of morpholino (n=438, two-tailed, student's t-test,  
1662 \*p=2.95×10<sup>-7</sup>) and from individual knockdown of *setd5* (\*p=1.86×10<sup>-9</sup>) or *mosmo* (\*p= 3.34×10<sup>-</sup>  
1663 <sup>6</sup>), showing a synergistic effect of decreased dosage of the homologs towards neuronal

1664 phenotypes. **(C)** Normalized axon length of *X. laevis* tadpoles with simultaneous knockdown of  
1665 *polr3e* and *setd5* showed no change in axon length (two-tailed student's t-test,  $p > 0.05$ ). In each  
1666 case, the individual knockdown was normalized and compared to the control injected with the  
1667 same amount of morpholino. Boxplots represent all data points with median, 25th and 75th  
1668 percentiles. Statistical details, including sample size, confidence intervals and p-values, are  
1669 provided in **S6 File**.

1670

1671 **S21 Fig. 16p11.2 genes exhibit higher phenotypic scores than 16p12.1 genes and are more**  
1672 **connected to each other than to other genes in the genome.** **(A)** Pairwise eye-specific  
1673 knockdown of 16p11.2 homologs (*rl*, *CG10465* and *Pp4-19C* crossed with other 16p11.2  
1674 homologs) lead to more severe phenotypic scores compared to pairwise interactions of 16p12.1  
1675 homologs ( $n=36$  for 16p11.2,  $n=12$  for 16p12.1, one-tailed Mann-Whitney,  $*p=3.51 \times 10^{-5}$ ). Grey  
1676 circles represent pairwise interactions, while 16p11.2 and 16p12.1 single-homolog knockdowns  
1677 are represented in orange and green, respectively. **(B)** Analysis of a human brain-specific  
1678 network shows higher average pairwise connectivity, measured as the inverse of the shortest path  
1679 between two genes, between pairs of 16p11.2 genes compared to the connectivity of 16p11.2  
1680 genes to the rest of the genome ( $n=25$  two-tailed Mann-Whitney,  $*p=6.64 \times 10^{-3}$ ). This trend was  
1681 not observed for 16p12.1 genes ( $n=6$ ,  $p > 0.05$ ). Boxplots represent all data points with median,  
1682 25th and 75th percentiles. Statistical details are provided in **S6 File**.

1683

1684 **S1 Table. *Drosophila* and *X. laevis* homologs of 16p12.1 genes.**

1685 DIOPT (24) and reciprocal BLAST (80) searches were used to identify fly homologs of 16p12.1  
1686 genes. The expression of homologs in the larval central nervous system during development was  
1687 assessed using FlyAtlas Anatomy microarray expression data from FlyBase (81).

1688

1689 **S2 Table. Number of experiments and genetic interactions identified in this study.**

1690 This table lists the number of crosses, RNAi/mutant/overexpression lines, tested pairwise  
1691 combination of genes, and genes that significantly enhanced or suppressed the phenotype of  
1692 16p12.1 homologs (**S2A Table**). The number of confirmed and potential negative and positive  
1693 genetic interactions towards eye phenotypes using the multiplicative model is also provided (**S2B**  
1694 **Table**).

1695

1696 **S3 Table. Hypotheses, experimental design, and conclusions obtained for experiments**  
1697 **performed in our study.**

1698 Explanation of hypotheses, experimental design, results, and conclusions that can be drawn or  
1699 hypotheses that can be further tested for each experiment performed in this study is provided.

1700

1701 **S4 Table. “Second-hit” variants identified in families with 16p12.1 deletion and tested for**  
1702 **interactions with 16p12.1 homologs.**

1703 Genes carrying “second-hits” were previously identified (9) through exome sequencing and SNP  
1704 microarrays in 15 children with the 16p12.1 deletion, and selected as disease-associated genes  
1705 carrying rare (ExAC frequency  $\leq 1\%$ ) copy-number variants, loss-of-function (frameshift,  
1706 stopgain or splicing) mutations, or *de novo* or likely-pathogenic (Phred-like CADD  $\geq 25$ )  
1707 missense mutations.

1708

1709 **S5 Table. Phenotypes observed for individual 16p12.1 homologs in *Drosophila* and *X. laevis***  
1710 **models.**

1711 Developmental and neuronal phenotypes observed with individual knockdown of 16p12.1  
1712 homologs in *Drosophila* and *X. laevis*.

1713

1714 **S6 Table. Sequences of oligonucleotides used for confirming gene knockdown in *Drosophila***  
1715 **and *X. laevis*.**

1716

1717 **S7 Table. *X. laevis* morpholino sequences used in this study.**

1718

1719 **S1 File. Stock list and genotypes of *Drosophila* lines used in the study (Excel file).**

1720 This file details genotypes of tissue-specific drivers, and stock centers, stock numbers and  
1721 genotypes of RNAi used to knock down the four 16p12.1 homologs, as well as RNAi, mutant, or  
1722 overexpression lines for homologs of “second-hit” genes and genes within conserved  
1723 neurodevelopmental pathways. Genotypes of recombinant lines of 16p12.1 homologs crossed  
1724 with interacting genes are also detailed, as well as the individual controls used for each  
1725 experiment. Details of the number of homologs, fly lines, and crosses used for all interaction  
1726 experiments are also provided. BDSC: Bloomington *Drosophila* Stock Center, VDRC: Vienna  
1727 *Drosophila* Stock Center.

1728

1729 **S2 File. Differentially expressed genes and Gene Ontology enrichments for knockdown of**  
1730 **16p12.1 homologs (Excel file).**

1731 List of differentially expressed genes, defined as log-fold change >1 or <-1 and false discovery  
1732 rate (FDR) <0.05 (Benjamini-Hochberg correction), following RNA sequencing of *Drosophila*  
1733 fly heads with *Elav-GAL4*-mediated knockdown of the four 16p12.1 homologs. Human  
1734 homologs of differentially-expressed fly genes were identified using DIOPT (24). Enriched Gene  
1735 Ontology (GO) and PantherDB terms are also provided for differentially-expressed fly genes and  
1736 their human homologs.

1737

1738 **S3 File. Summary of genetic interactions identified with 16p12.1 homologs in *Drosophila***  
1739 **(Excel file).**

1740 This file details the genes that modulated the phenotypes of the 16p12.1 homologs, as well as the  
1741 genetic interactions identified in this study.

1742

1743 **S4 File. Interaction scores and observed and expected values for all tested genetic**  
1744 **interactions of 16p12.1 homologs in *Drosophila* (Excel file).**

1745

1746 **S5 File. Connectors of 16p12.1 and 16p11.2 genes identified in a human brain network**  
1747 **(Excel file).**

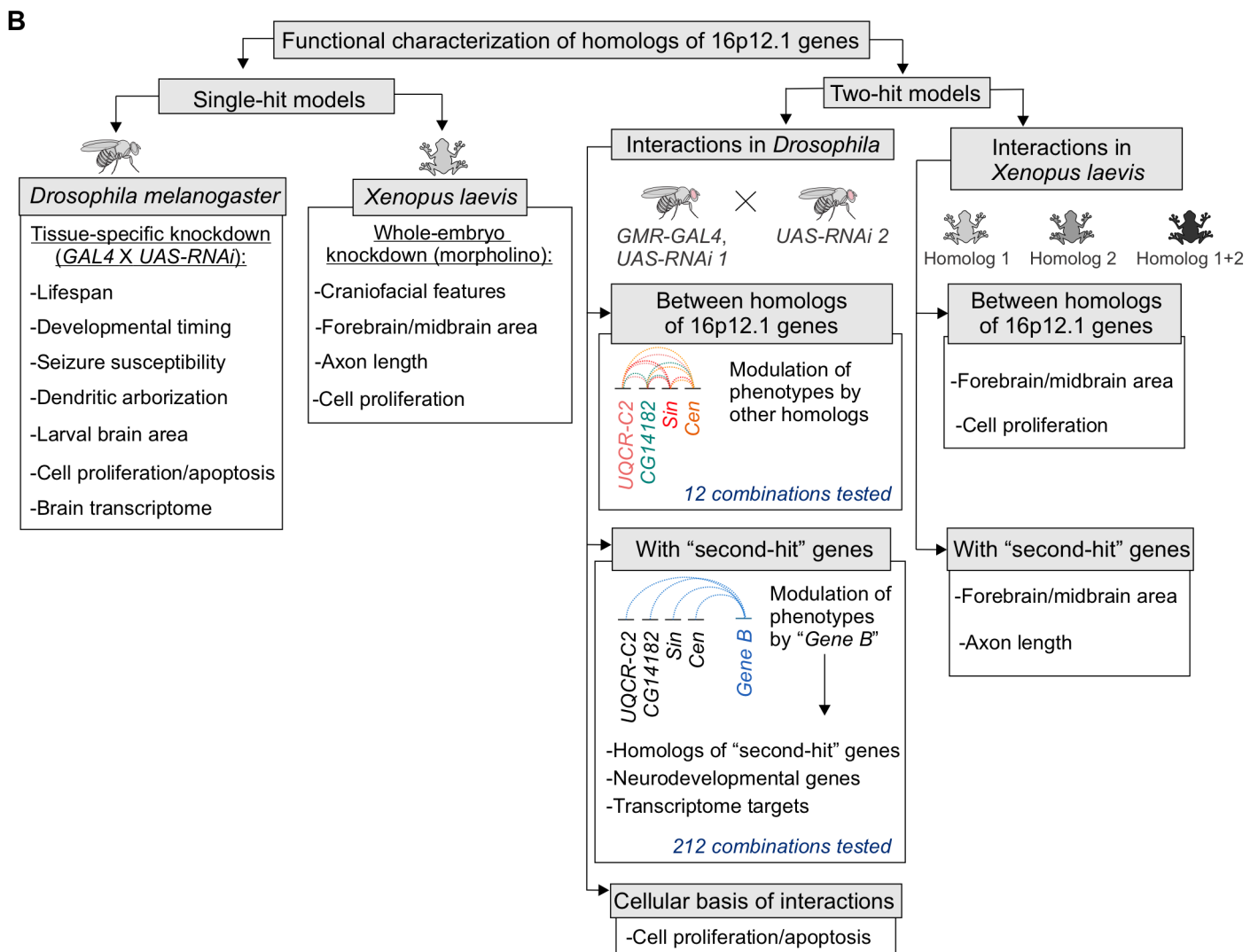
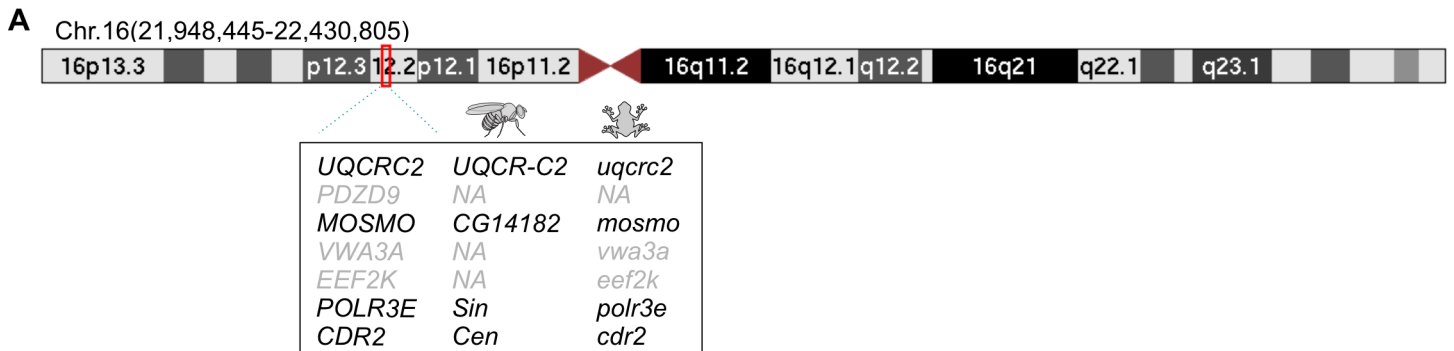
1748

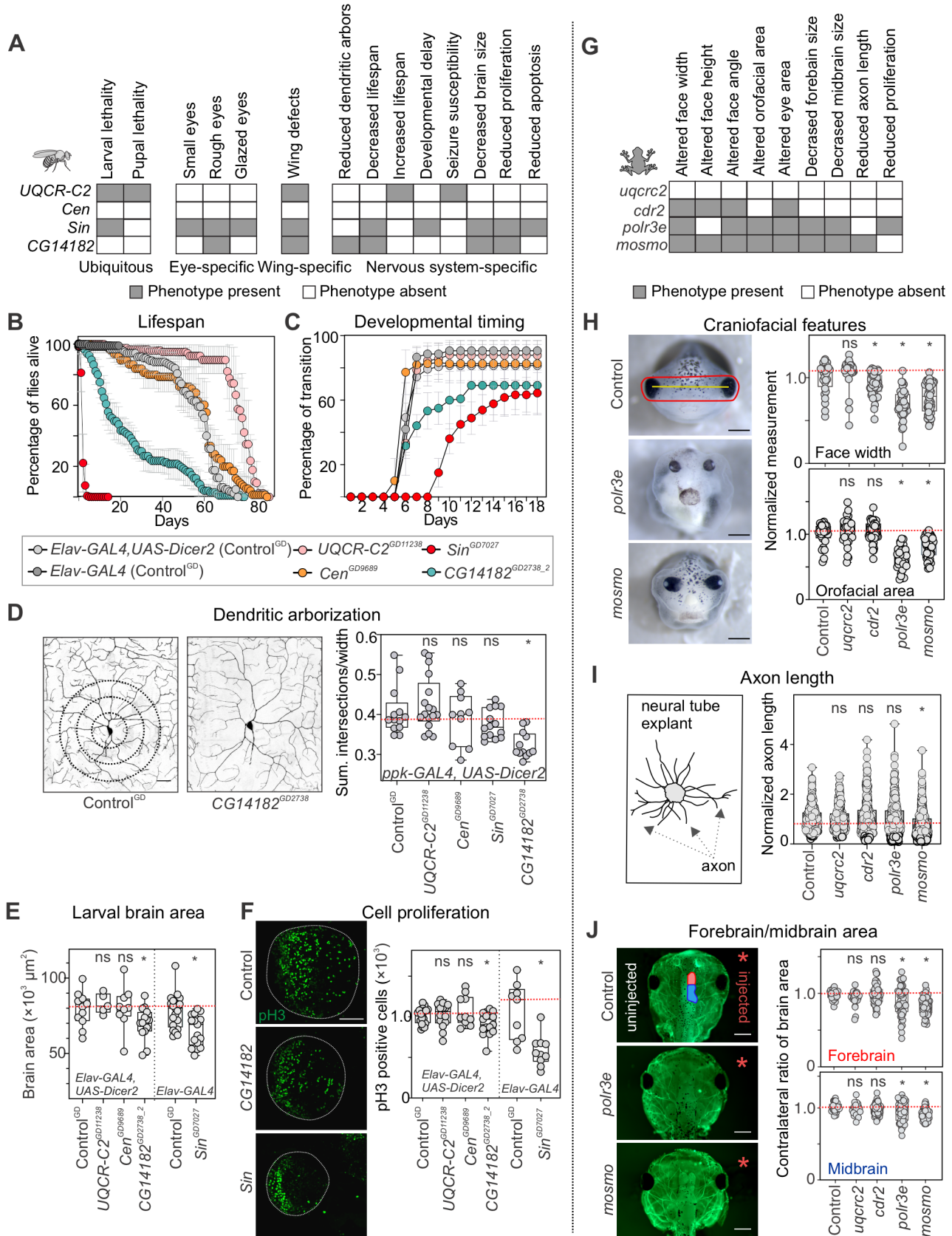
1749 **S6 File. Statistical analysis of experimental data (Excel file).**

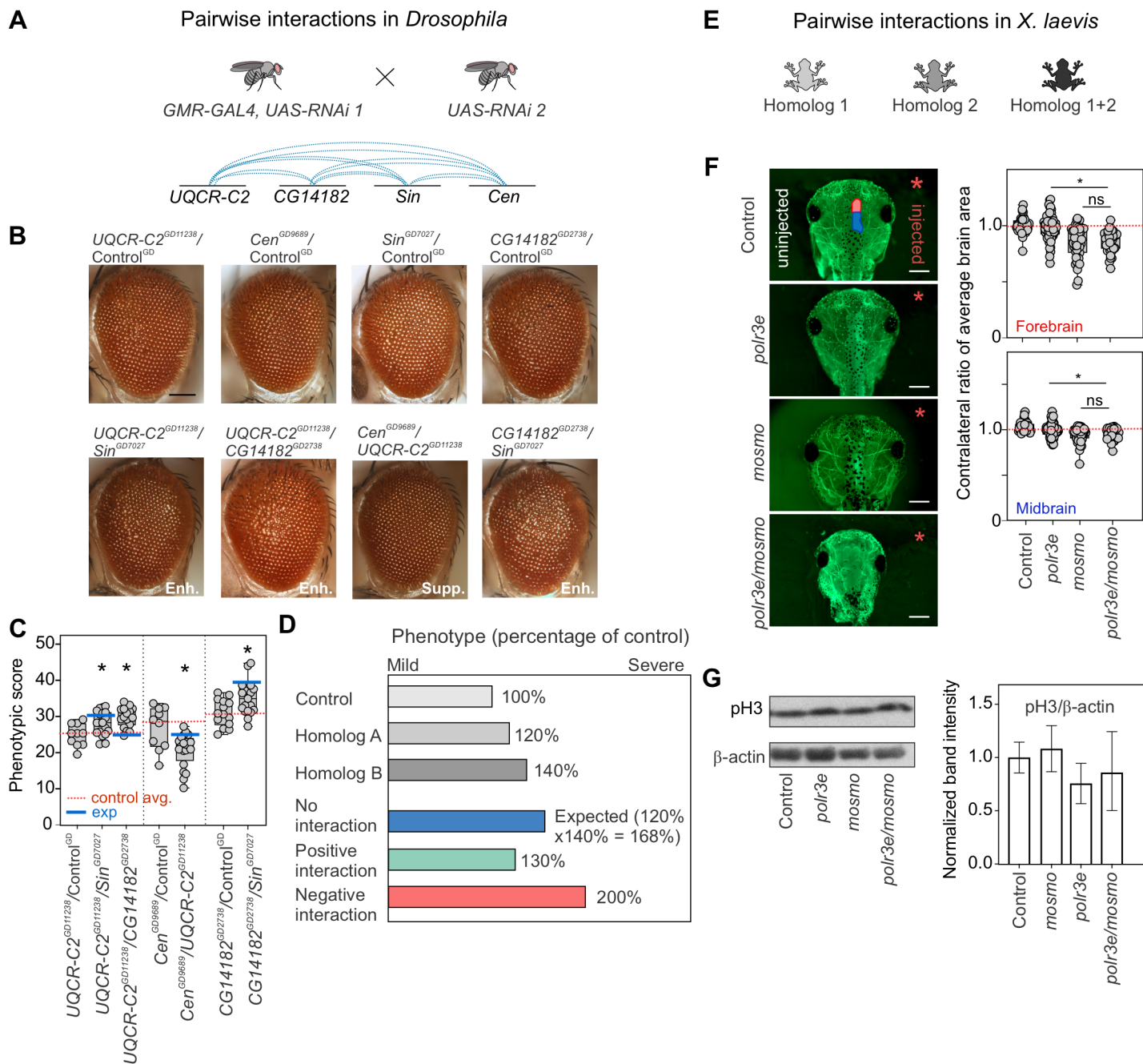
1750 This file provides details of all statistical information, including sample size, test statistics, p-  
1751 values, and Benjamini-Hochberg FDR corrections for all data shown in the main and  
1752 supplemental figures. Details for ANOVA tests include factors, degrees of freedom, tests  
1753 statistics, and post-hoc pairwise t-tests with Benjamini-Hochberg FDR corrections.

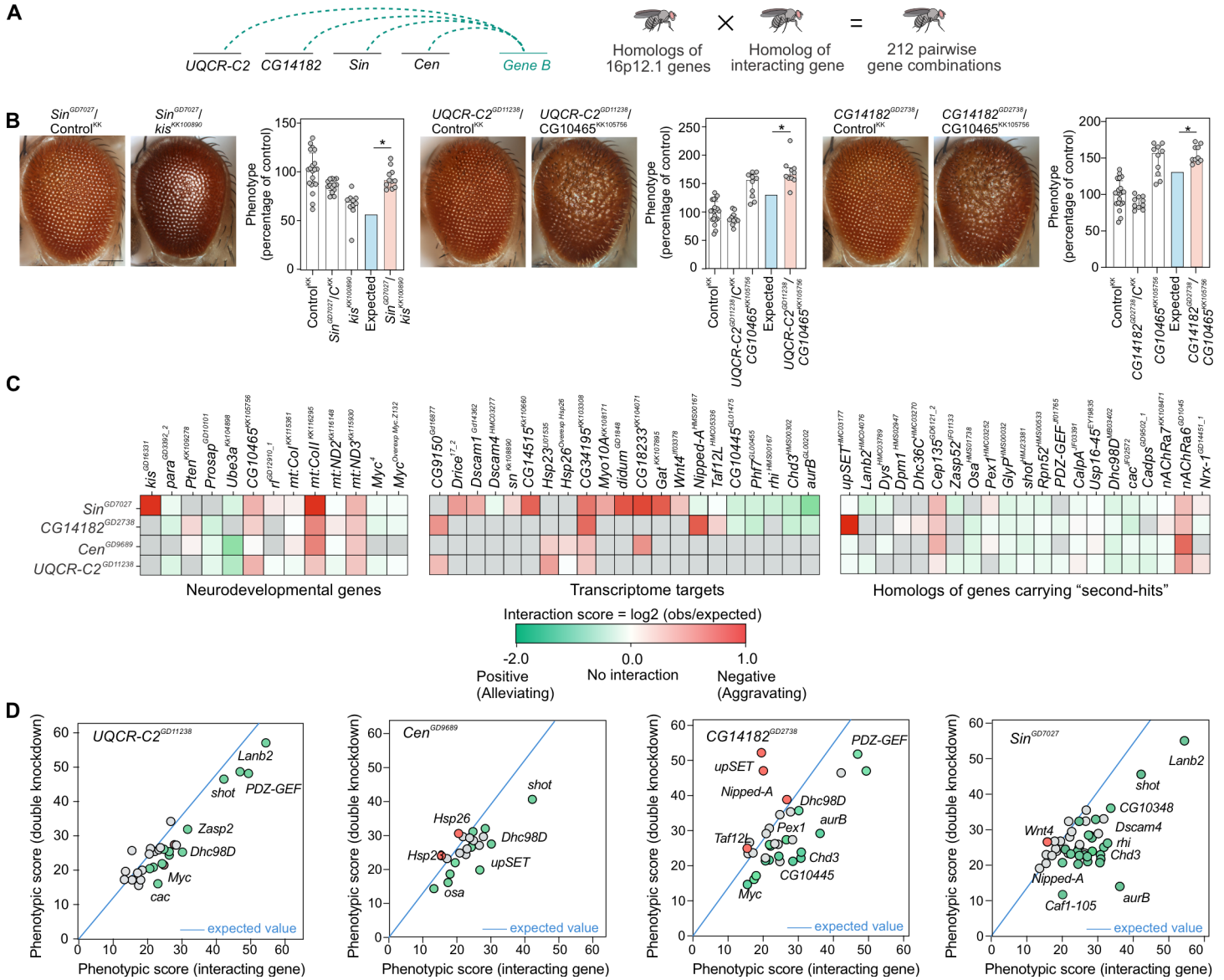
1754



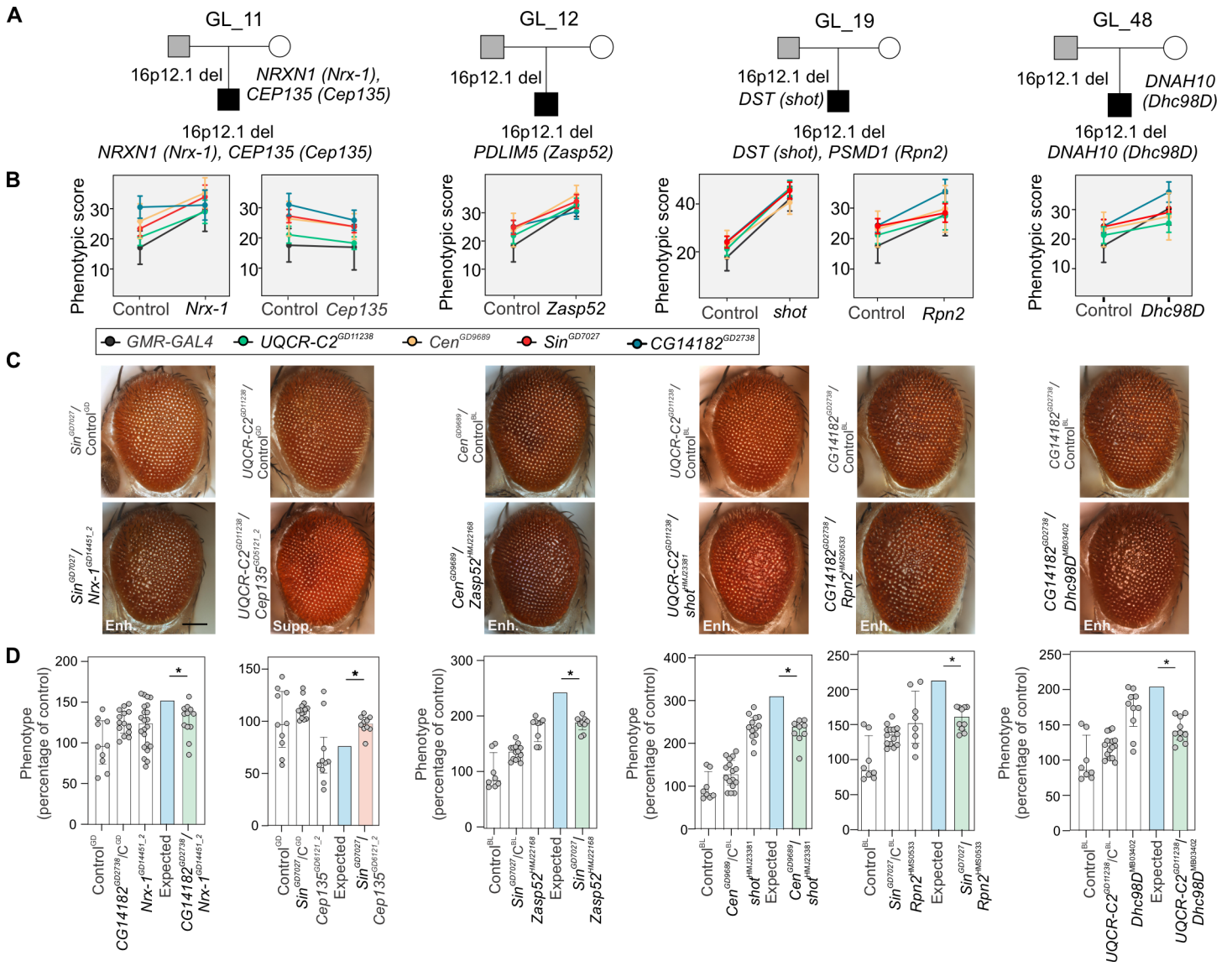




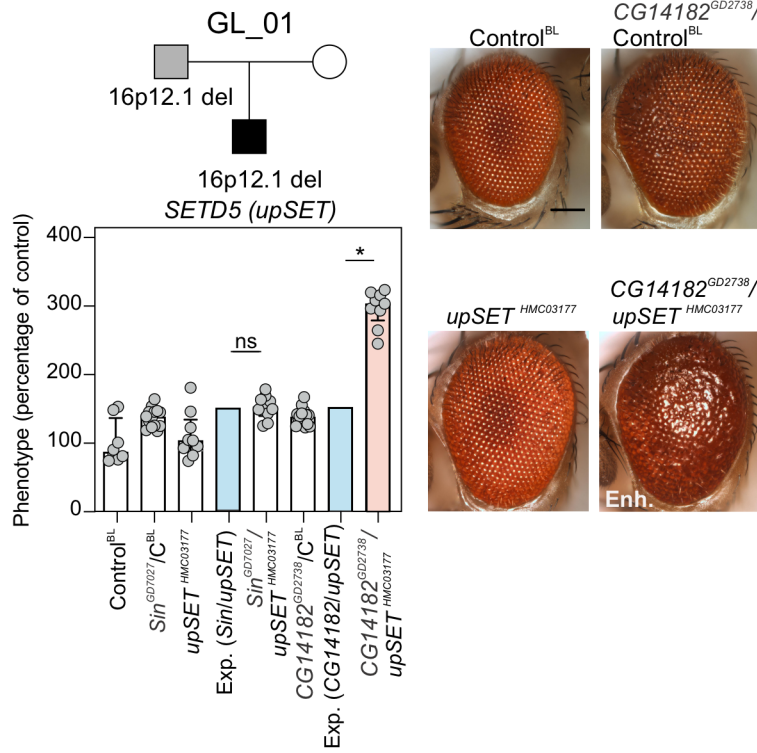




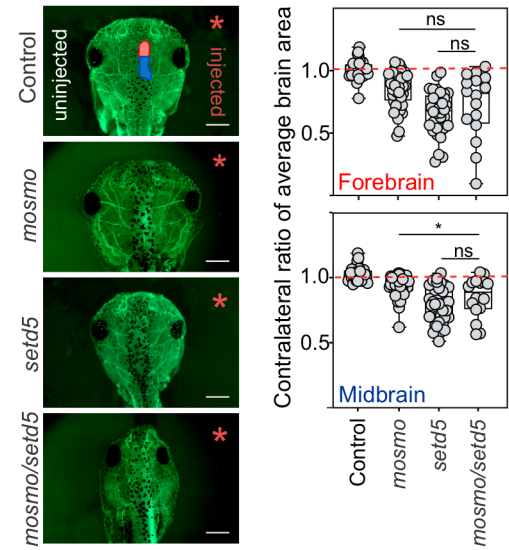
Interactions of 16p12.1 homologs with patient-specific “second-hits”



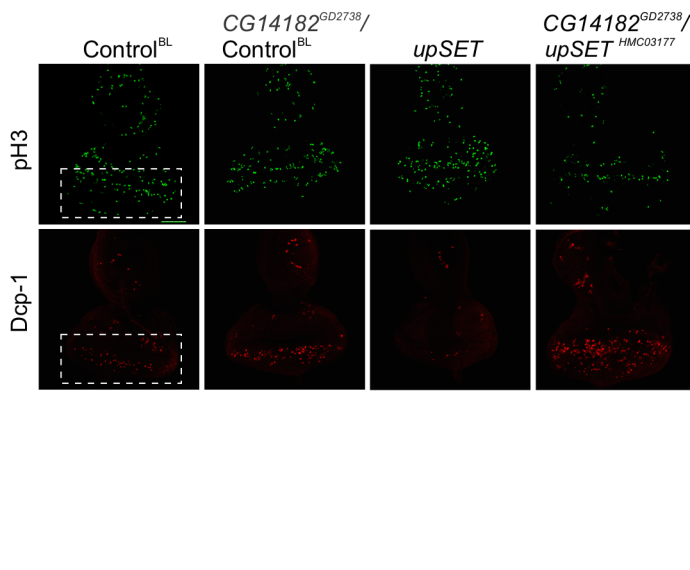
### A Patient-specific "second-hit" interaction in flies



### C Forebrain/midbrain area



### B Cell proliferation/apoptosis



### D Axon length

